A Whole-Mission, Simulation-Based Parametric Analysis and Design Approach for the RFA TWO Reusable Space Launch System

Rory Dick

Thesis for the Degree of Master of Science in Astronautics and Space Engineering

Cranfield School of Aerospace, Transport and Manufacturing

In collaboration with Rocket Factory Augsburg AG

A Whole-Mission, Simulation-Based Parametric Analysis and Design Approach for the RFA TWO Reusable Space Launch System

A thesis submitted in partial fulfilment of the requirements for the degree of

Master of Science in Astronautics and Space Engineering

Submitted by:

Rory Dick

Supervisors:

[redacted]

School of Aerospace, Transport and Manufacturing

Cranfield University

20th August 2024

[redacted]

Abstract

Commercial space mission analysis and launch vehicle sizing tools used in the preliminary design phase of space launch systems cannot be directly applied to the analysis and design of non-traditional reusable or partially reusable launch systems, due to the absence of specialised retro-propulsive landing algorithms within their standard libraries. The landing phase of the mission is integral to the recovery and reuse aspect of next-generation, partially-reusable launch systems such as those under development at Rocket Factory Augsburg (RFA). The output of this project provides RFA with the ability to [redacted] An end-to-end simulator for reusable launch vehicles was developed with particular focus on the landing module, which incorporates state-of-the-art convex programming methods to generate retro-propulsive landing trajectories that are guaranteed to minimise propellant consumption with high reliability. The simulator is provided to RFA for the purpose of [redacted] A basic demonstration of an approach for carrying out [redacted] is included in this project in the form of a parametric analysis and design study, which found several advisory [redacted]

Acknowledgments

In memory of RFA ONE S1VE

Contents

List of Figures

List of Tables

Nomenclature

AG	Aktiengesellschaft (public limited company)
[redacted]	[redacted]
CFD	Computational fluid dynamics
CoM	Centre of mass
ConOps	Concept of operations
CVXPY	Convex, Python
DATCOM	Data compendium
DCP	Disciplined convex programming
ECEF	Earth-centred, Earth-fixed
ECO	Engine cut-off
ESA	European Space Agency
GNC	Guidance, navigation and control
IPM	Interior point method
LOx	Liquid oxygen
MoI	Moment of inertia
MPC	Model-predictive control
MSV	Maximum staging velocity
NASA	National Aeronautics and Space Administration
[redacted]	[redacted]
NRLMSISE-00	Naval Research Laboratory Mass Spectrometer and Incoherent Scatter Radar, Exosphere, 2000
OTV	Orbital transfer vehicle
PID	Proportional, integral, derivative
RASAero	Rogers Aero Science Aerodynamic
RCS	Reaction control system
RFA	Rocket Factory Augsburg
RK45	Runge-Kutta, order 5(4)
RL	Reinforcement learning
RP-1	Rocket propellant 1

RTLS	Return-to-launch-site
SSO	Sun-synchronous orbit
TRL	Technology readiness level
TVC	Thrust vector control
UEN	Up-East-North
US	United States

1

Background and Literature Review

This section introduces the underlying context for the project, including key information about space launch system company Rocket Factory Augsburg (RFA) and the launch systems it has been developing since its incorporation. Included are details of how these launch systems evolved and how they fit into the wider European and international commercial space transportation landscape.

In addition, this section presents the problem that this project tackles and its relevance to the development of RFA's next-generation launch system, RFA TWO.

1.1 Project Introduction

This project, entitled "A Whole-Mission, Simulation-Based Parametric Analysis and Design Approach for the RFA TWO Reusable Space Launch System", is an individual research endeavour conducted by Mr. Rory Dick of Cranfield University, Bedfordshire, United Kingdom. The project was delivered in partial fulfilment of the requirements for the degree of Master of Science in Astronautics and Space Engineering, and was conducted in collaboration with Rocket Factory Augsburg AG via a working student contract agreement.

The project addresses [redacted] RFA TWO launch system due to a [redacted] to generate proven propellant-optimal booster landing trajectories within [redacted] engineering simulation and analysis pipelines.

1.2 Important Definitions

1.2.1 "Booster"

Space literature often reserves the word "booster" to describe solid-propelled, expendable rocket boosters such as those jettisoned during the ascent of many orbital launch vehicles. In Europe especially, the word is also used to describe the "first stage" or "core stage" of a launch vehicle - typically the largest stage and the first to fire. It is this definition that is used in this document.

1.2.2 "Trajectory"

The word "trajectory" is used frequently throughout this document. "Trajectory" here will refer not only to the position history of a rocket across a given phase of flight, but also to the history of all other relevant parameters of the rocket in question. In other words, "trajectory" is used to describe the full *state* of the rocket, not just its position.

In mathematical terms, for example:

$$Trajectory \equiv [\mathbf{r} \quad \mathbf{v} \quad t \quad m \quad \mathbf{T} \quad \theta \quad (\dots)]^\top \tag{1.1}$$

where $\mathbf{r}$ is the rocket position vector, $\mathbf{v}$ is the velocity vector, t is time, m is the vehicle mass, $\mathbf{T}$ is the thrust vector, and θ is an attitude angle.

1.3 Rocket Factory Augsburg

RFA is a private company developing orbital space launch systems, headquartered in Augsburg, Bavaria. The company has design, manufacturing, test and launch sites in Germany, Scotland, Portugal and Sweden. Since its incorporation in 2018, RFA's efforts have been centred around the RFA ONE launch system[1], which includes a three-stage, kerolox, staged combustion cycle launch vehicle and its launch site in the Shetland Islands of Scotland, United Kingdom.

1.4 RFA Space Systems

RFA's launch system development activities are conducted in close alignment with [redacted] Outside of upstream ESA requirements, other drivers influencing the design of RFA's systems include [redacted]. By the time all

of these factors are considered, the set of all possible design configurations for a new space launch system can effectively be reduced to a few concepts that make economic and technological sense.

The company's entry-level launch system, RFA ONE, is the continuation of one such concept and is in the [redacted] phase as of [redacted], expected to reach orbit in [redacted]. A [redacted], next-generation platform, RFA TWO, is [redacted] and is the focus of this project. Figure 1.1 shows a scale comparison between RFA ONE and an impression of RFA TWO.

(a) RFA ONE

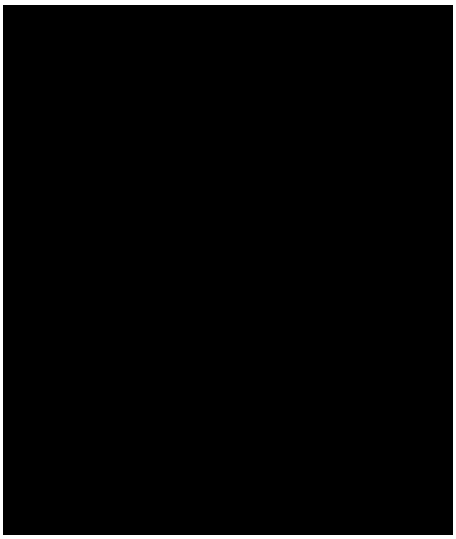

(b) RFA TWO
not actual design

Figure 1.1: Scale comparison between RFA ONE and RFA TWO

1.4.1 RFA ONE

RFA ONE is developed to [redacted] The system is also [redacted]

The vehicle itself is expendable and [redacted] launch from SaxaVord Spaceport[2] on the Shetland Islands of Scotland, United Kingdom. This launch site was chosen due to [redacted] Some specifications of a nominal configuration of RFA ONE are shown in Table 1.1

Table 1.1: RFA ONE launch vehicle nominal specifications

Parameter	**Value**
Number of stages	3
Overall length	[redacted] m
Tank diameter	[redacted] m
Number of first stage engines	9
Number of second stage engines	1 or 2
Gross lift-off mass	[redacted] kg
Dry mass	[redacted] kg
Theoretical payload mass to nominal orbit	[redacted] kg
Propellants	RP-1/LOx
Engine cycle	[redacted] staged combustion
Lift-off thrust	[redacted] kN
Lift-off thrust-to-weight	[redacted]
Nominal orbit	[redacted]

1.4.2 Helix Rocket Propulsion Systems

The development and test of an orbital-class rocket engine is a hallmark of a serious contributor in the space launch sector. At most, there are seven European companies who have achieved this critical milestone as of September 2025, with RFA being one of them.

RFA's "Helix" series of rocket engines and associated propulsion systems[3] is the first example of a staged combustion cycle platform to come out of an ESA Member State. 9 first-generation Helix engines will be used on the booster stages of [redacted] the system is in constant development and [redacted] will be deployed on [redacted] RFA ONE flights [redacted]. Since this project focuses on future launch systems, the nominal Helix [redacted] specifications are given here in Table 1.2.

Table 1.2: [redacted] propulsion system nominal specifications

Parameter	Value
Fuel	[redacted]
Oxidiser	[redacted]
Sea-level thrust	[redacted] kN
Vacuum specific impulse (I_{sp})	[redacted] s
Vacuum thrust	[redacted] kN
Thrust-to-weight	[redacted]
Chamber pressure	[redacted] bar

1.4.3 Redshift Orbital Transfer Vehicle

The Redshift orbital transfer vehicle (OTV) is RFA's proprietary orbital stage[4] which uses RFA's Fenix multi-ignition in-space eco bi-propellant propulsion system. Redshift is capable of deploying and hosting several independent payloads on the same mission with different orbital parameters, changing its inclination and orbital axes as necessary. A render of the Redshift OTV is shown in Figure 1.2.

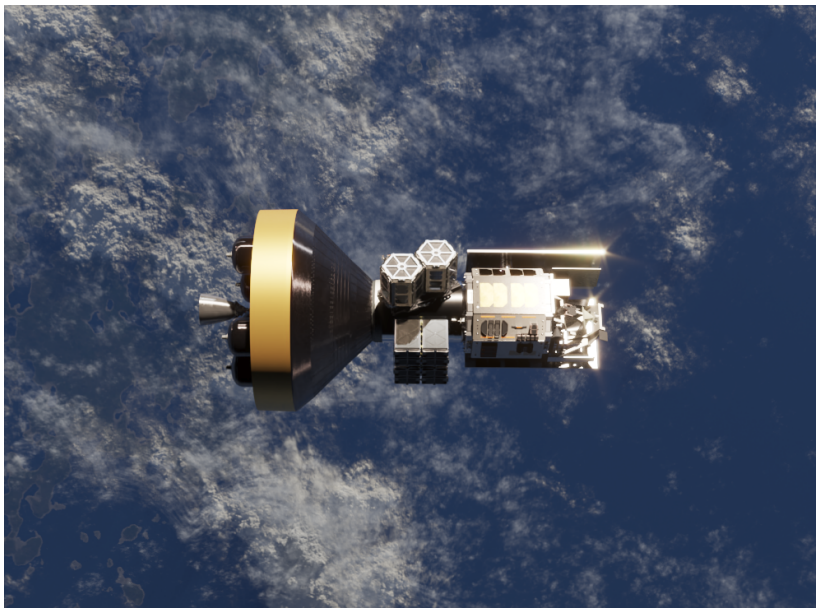

Figure 1.2: Render of a RFA Redshift orbital transfer vehicle hosting various payloads

Much like the Helix series, the first generation of Redshift has been successfully qualified and is used on RFA ONE, while [redacted] for RFA TWO satellite deployment missions. Some nominal specifications of the Redshift [redacted] are provided in Table 1.3.

Table 1.3: [redacted] orbital transfer vehicle nominal specifications

Parameter	**Value**
Length	[redacted] m
Diameter	[redacted] m
Wet mass	[redacted] kg
Dry mass (excluding payloads)	[redacted] kg
Engines	[redacted] RFA Fenix
Propellants	Eco bi-propellant
Vacuum specific impulse (I_{sp})	[redacted] s
Vacuum thrust	[redacted] kN

1.4.4 Argo Pressurised Capsule

In addition to the Redshift OTV, an alternative proprietary upper-stage option for next-generation RFA vehicles is the Argo pressurised capsule[5]. Argo is designed to transport crew and cargo on various mission types including space station rendezvous and docking. It is fully reusable - capable of atmospheric re-entry using an inflatable decelerator. Figure 1.3 shows a render of the Argo pressurised capsule in orbit, while some high-level specifications of the system are provided in Table 1.4.

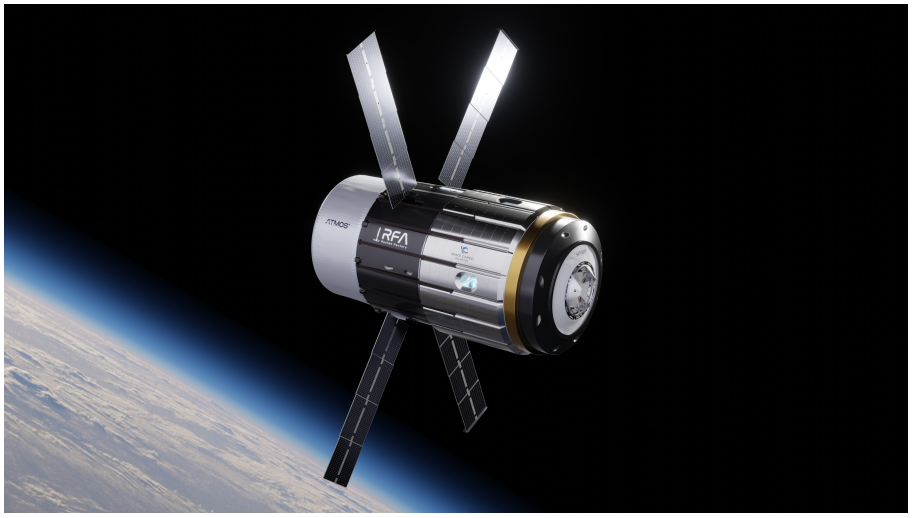

Figure 1.3: Render of a RFA Argo pressurised capsule

Table 1.4: Argo pressurised capsule high-level specifications

Parameter	**Value**
Length	[redacted] m
Diameter	[redacted] m
Wet mass	[redacted] kg
Dry mass (excluding cargo)	[redacted] kg
Payload mass	[redacted] kg up, [redacted] kg down
Pressurised volume	[redacted] m^3
Peak power generation	[redacted] kW
Propulsion	[redacted] RFA Fenix eco bi-propellant
Reaction control	[redacted]

1.4.5 RFA TWO

RFA TWO builds upon many of the technologies that the company has been able to mature over the course of the development of RFA ONE, including the Helix engine, [redacted], [redacted] and [redacted]. [redacted] there are many significant differences.

In addition to the obvious increase in size as evident in Figure 1.1, the principal engineering challenge of RFA TWO is that of booster recovery and reuse. Several companies have now proven that recovery and reuse of space hardware is possible and commercially advantageous[6], prompting the ESA strategy to tend towards a new paradigm of reusable launch systems due to the great cost savings and reduction of environmental harm, both terrestrially and in space.

RFA TWO is emergent of this paradigm shift - the development of a larger, more performant launch system which incorporates aspects of reusability was decided as the correct path to pursue in order to [redacted] for RFA moving forward.

[redacted] objectives are defined for the nominal system. Some of the objectives with relevance to this project are listed in Table 1.5.

Table 1.5: Relevant RFA TWO [redacted] objectives

ID	Objective
01	[redacted]
02	[redacted] the RFA TWO booster stage should be recoverable and usable for more than 1 flight
03	The RFA TWO launch system should be capable of a nominal launch cadence of [redacted]
04	The RFA TWO launch system vehicle should be capable of hosting a RFA Argo pressurised, human-rated capsule as its upper stage
05	The recurring cost of the RFA TWO launch system should remain [redacted]
06	The RFA TWO booster stage should propel [redacted] to a state where they are capable of carrying out their mission as the primary objective
07	The RFA TWO booster stage should safely perform a controlled landing at a specified location as the secondary objective
08	The nominal RFA TWO launch system should be optimised for [redacted]

1.5 Problem Statement

With reference to NASA and ESA space project life cycle standards[7], phases are defined for the development, operation and disposal of a space system as shown in Table 1.6.

Table 1.6: Typical space project life cycle phases

Project phase	Activities
Pre-phase A	concept and feasibility studies
Phase A	concept and technology development
Phase B	preliminary design and technology completion
Phase C	final design and fabrication
Phase D	system assembly, integration and test, launch and checkout
Phase E	operations and sustainment
Phase F	close-out and disposal

During Phase A/B of the process it is common, especially for launch systems, to make use of spacecraft "sizing" tools which, given a set of boundary conditions, are able to output a vehicle configuration which is optimal with respect to some criteria. These tools are commercially available or can be developed specifically for a project or series

of projects. [redacted] - to refine the configurations and parameters of [redacted] launch vehicles.

[redacted] is a high-fidelity, 6 degree-of-freedom mission simulator which incorporates accurate environmental models and can simulate high-order dynamics. Any number of boundary conditions and constraints can be defined as required for the specifics of a mission, while any parameters not explicitly defined can be "solved for" by [redacted]. In the case of RFA ONE, for example, where the sizing, design and performance of the launch system is [redacted] fully defined, [redacted] could output a set of possible mission or trajectory profiles for that launch system which satisfy some optimality criteria. Alternatively, for example, if a desired nominal orbit and launch site is known but only a few basic parameters of the launch system are defined, [redacted] can generate remaining unknown vehicle or launch site parameters which would result in a launch system capable of conducting the desired mission.

[redacted] crucial in optimising space system designs, especially for launch vehicles, where small margins can make the difference between commercial success and failure. However, in addition to the high computational effort required to run them, a major issue is presented when tools like [redacted] are relied upon for [redacted]: there is no built-in functionality to properly model the recovery aspect of the mission. Certainly, [redacted] is not designed for such missions and does not guarantee the generation of suitable landing trajectories.

The reason for this is that the algorithms used to generate landing profiles in [redacted] are the same ones used to generate ascent trajectories, and are the result of some generalised optimisation approach. [redacted] is a closed-source "black box" with no possibility to inspect the algorithms used, but it can be reasonably asserted that the types of highly specialised logic that would be deployed on flight hardware for retro-propulsive landing in the real case are not included in the pipeline.

Given the fact that the user is able to provide any initial and final state vector for the launch vehicle in question, it is *technically* possible to "brute force" [redacted], making it produce a recovery or landing trajectory by specifying a final state vector at the desired landing location with near-zero velocity and an upright booster orientation. Even though these landing profiles are likely to be feasible and may even be close to propellant-optimal, the point is that the algorithm used by the tool is not possible to validate for deployment on near-real-time flight systems in the domain of retro-propulsive landing.

As a result, the vehicle sizing parameters and configurations output [redacted] in isolation are not guaranteed for optimality with respect to the full mission profile of a reusable space launch system since there is uncertainty in the landing profile, a key aspect of the mission which requires great attention.

1.6 Project Aims

The primary aim of this project was to address the [redacted] problem by developing an end-to-end simulator for RFA TWO and other reusable space launch systems which incorporates the ascent, manoeuvre and landing phases of the mission. The main contribution is the landing phase, where a propellant-optimal landing guidance algorithm of the type appropriate for real-time deployment is included in order to generate landing profiles close to what would be suitable for real recoveries of the RFA TWO booster stage. With this whole-mission, simulation-based approach it is possible for RFA to [redacted] of RFA TWO with confidence that the the overall launcher performance across the whole mission is well understood.

A secondary aim was to deliver [redacted] the current RFA TWO baseline configuration, produced based on the application of the simulator to a basic parametric analysis and design study of RFA TWO, centred around the expected nominal operating point of the launch system.

2

Methodology

This section presents the general approach taken to achieve the aims of the project, including the rationale and trade-offs associated with this approach. The scope and basic functionality of the simulator for various use cases is presented, and the method used to [redacted] for RFA TWO using the simulator is discussed.

2.1 Whole-Mission Simulation

To achieve the project aims, a simulator was developed which allows for parametric analysis of the booster trajectory across the full mission, with emphasis on the landing phase - a phase of flight where [redacted] characterise the system performance with accuracy. The simulator functions like a digital twin of the RFA TWO booster, allowing design changes to be made digitally for the purpose of assessing the resulting change in performance.

2.2 Simulator Design Priorities and Limitations

It is important to note that the simulator is not designed to prioritise accuracy of the vehicle's *spatial* state across the phases of the mission. [redacted] and other tools are capable of modelling mission profiles with very high spatial fidelity for use cases such as characterisation of orbital injection performance. Development of a system capable of matching this spatial precision across vehicle ascent and in-space manoeuvring was not within the scope of this project.

Though spatial parameters are captured with reasonable accuracy within the simulator, its core priority is to act as a tool for optimisation of the vehicle design, sizing and configuration, with the landing phase of the mission fully accounted for. Therefore, design parameters such as vehicle mass, allowable structural and thermal loads, thrust, and thrust-vector control (TVC) gimbal angle bounds are of greater interest in the output

than the precise spatial state of the vehicle at any discrete point.

2.2.1 Scope

RFA TWO is expected to deliver a range of payload types, including the Argo pressurised, human-rated capsule (see Table 1.5, Objective ID 04). While the sizing and configuration of the RFA TWO booster stage [redacted] according to the mission objectives. For example, a [redacted] mission may carry an Argo capsule (see Subsection 1.4.4) as the third stage, while a [redacted] mission would carry a Redshift orbital transfer vehicle (see Subsection 1.4.3). For this reason, the simulator places emphasis on the granular parameterisation of the booster stage, while the overall vehicle performance, which includes the upper stages, is captured by extrapolating the upper stages' spatial state from the point of booster separation based on basic performance parameters such as their Delta-V values.

With the upper stages accounted for in this way, the scope of the simulator extends to the full concept of operations (ConOps) for the RFA TWO booster flight. Figure 2.1 shows the ConOps for a [redacted] landing of the RFA TWO booster stage, where it can be seen that the mission is divided into three main phases: ascent, manoeuvre, and landing. It is these phases that define the three modules of the simulator.

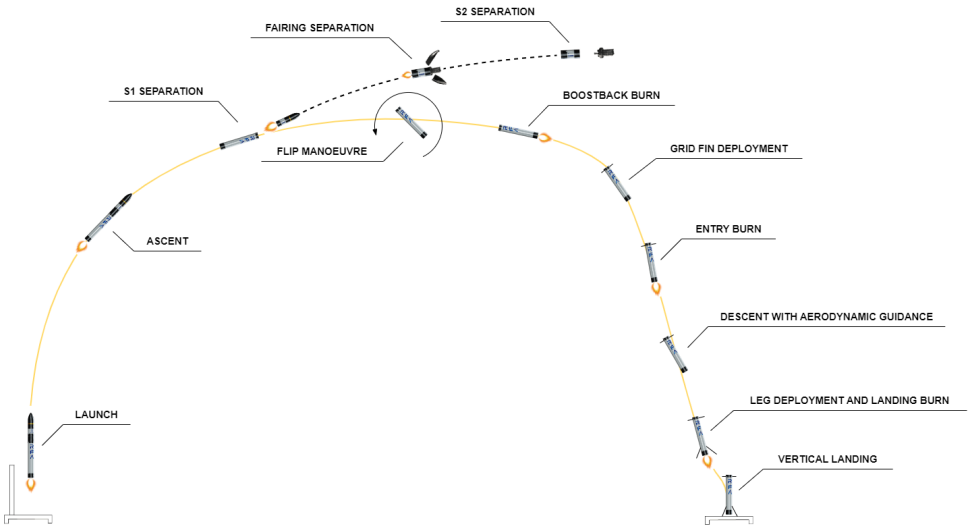

Figure 2.1: Concept of operations for RFA TWO [redacted] booster landing

2.3 Simulator Functional Architecture

The ascent, manoeuvre and landing modules of the simulator can be used concurrently for analysis of whole missions, or in isolation for assessment of a specific phase of flight. A

diagram of the functional architecture of the full concurrent simulator is shown in Figure 2.2, where the flow of data is shown by the arrowed lines.

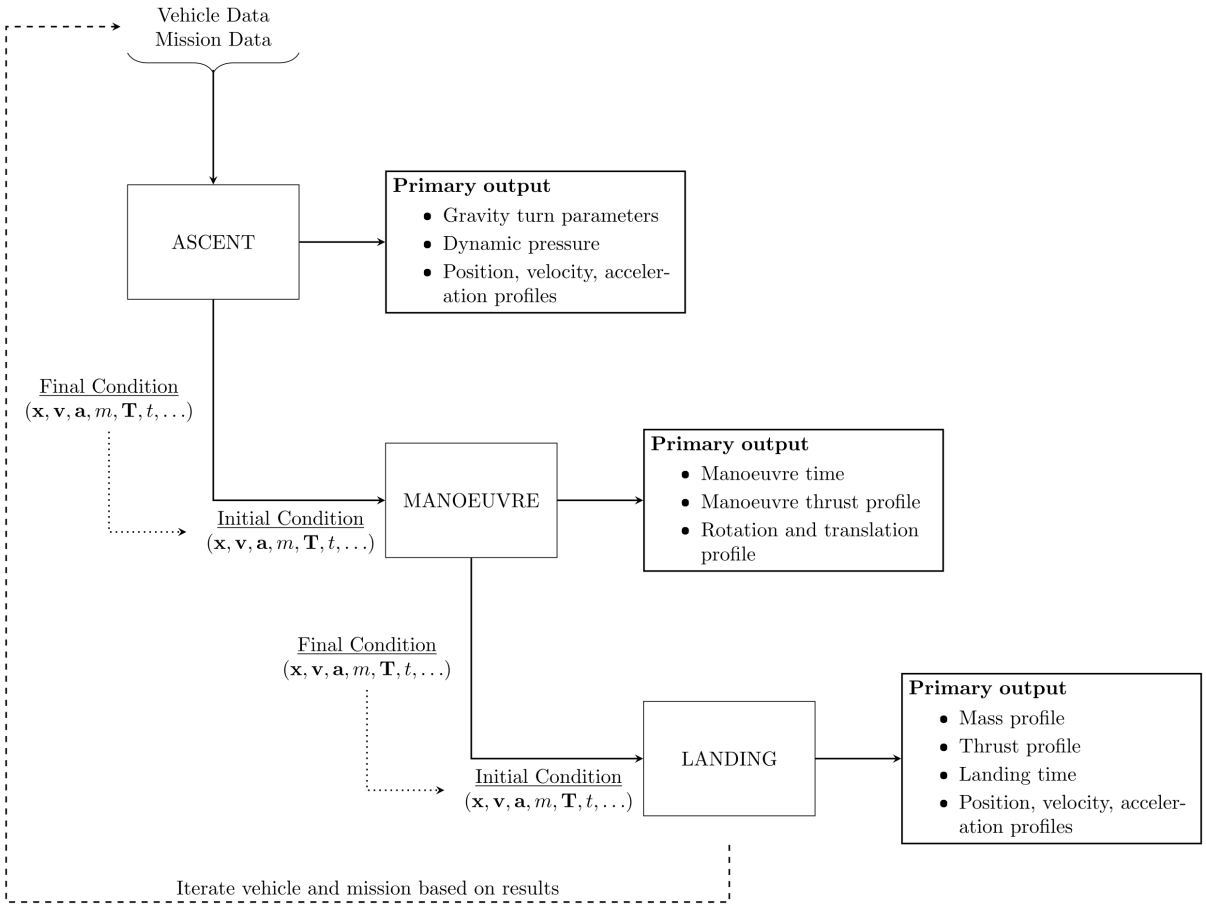

Figure 2.2: Simulator functional architecture diagram

The simulator requires the the provision of a base configuration of the launch vehicle, which represents the initial design that is to be assessed. In the case of RFA TWO, this initial design would come from the [redacted] estimate of the vehicle parameters required to insert [redacted], where these are driven by [redacted] and other [redacted] constraints. As a reminder, vehicle configurations output by [redacted] incorporate the landing phase of the mission poorly from an algorithmic standpoint and without consideration for factors relevant to reusable systems such as the extra mass of [redacted]. Despite this, [redacted] values are suitable and useful for an initial guess.

In addition to the vehicle parameters, some information about the desired mission profile is required to set up the simulator. This includes the desired landing site for the booster and the desired booster staging state, which can be defined as a specific altitude or velocity, or a maximum velocity regardless of altitude. The expected performance of the upper stage(s) should be taken into account when defining the desired staging state, ensuring that the staging conditions can feasibly result in mission success.

Table 2.1 contains the vehicle data and Table 2.2 contains the mission data that is to be provided as input to the simulator.

Table 2.1: Vehicle data input to run the full simulator

Vehicle Data
Fully-stacked vehicle & booster:
Acceleration limits
Aerodynamic data ($C_D(Mach), A_{ref}$)
Stage diameters
Dynamic pressure limits
Gross lift-off mass
Length
Booster only:
Burn time
Post-ascent centre of mass
Inert mass
Propellant mass
Post-ascent moment of inertia
Length
[redacted] thruster gain
[redacted] thruster [redacted]
Separation buffer time
Thrust (min, max)
Specific impulse

Table 2.2: Mission data input to run the full simulator

Mission Data
Vehicle initial flight path angle
Booster landing site position
Booster desired pre-landing attitude
Booster separation altitude (optional)
Booster separation velocity (optional)

The simulator ascent module generates a gravity turn trajectory which includes the full state (see Subsection 1.2.2) of the vehicle across the ascent. Iterative characterisation of the ascent performance of different vehicle configurations can be performed efficiently through isolated analyses of this ascent trajectory.

The final ascent condition of the booster can be taken as the initial state for the manoeuvre module of the simulator, which simulates the booster performing a planar rotation - decoupled from the translational motion - to meet a desired pre-landing attitude angle. The main output of the manoeuvre module is a rotation manoeuvre time and profile, along with the associated decoupled translation profile across the manoeuvre which is simply propagated via ballistic dynamics. The manoeuvre performance of different vehicle configurations can also be performed in isolation within the manoeuvre module, separate from the ascent and landing simulations.

The post-manoeuvre state vector can then be fed to the landing module which gen-

erates a propellant-optimal landing profile based on a specialised, tailored and robust optimisation algorithm. Similarly to the preceding modules, the trajectory generated by the landing module can be analysed in isolation or as part of the overall pipeline, and the landing can be simulated iteratively to gain an understanding of the effect of different designs on the landing performance. This represents the main contribution of the project and the highest-accuracy retro-propulsive landing simulator [redacted]

2.3.1 Landing Module in Combination with [redacted]

It is possible and advisable in some cases to combine the use of the landing module from this project with an ascent and manoeuvre profile from [redacted] in order to achieve higher spatial accuracy over the ascent and higher-fidelity post-ascent manoeuvre characterisation. However, [redacted] simulations can take many hours to run and require performance computing resources which are not always available. Iterating over several vehicle configurations could take many days. In contrast, an entire mission simulation using the simulator from this project runs in around two minutes on a modern workstation and produces ascent profiles with ballistic impact points within ±10% of [redacted] numbers for the same boundary conditions.

2.4 Application to RFA TWO

The main utility that RFA gains by using this simulator is [redacted] of RFA TWO. The simulator is useful because it allows the performance of prospective design changes to be assessed quickly and accurately, with confidence that the landing algorithm is representative of the type that will be deployed in the real case. Without this simulator, [redacted] to produce design configurations for RFA TWO, without any knowledge of the underling logic that [redacted] applies to generate flight profiles. Reliance on [redacted] of the RFA TWO launch system.

Two example workflows for application of the simulator to the analysis and design of RFA TWO are as follows:

Example 1: Optimisation of vehicle diameter

1. A base vehicle configuration from [redacted] is simulated, which generates a full mission profile including the trajectory (as defined in Subsection 1.2.2) across ascent, manoeuvre and landing of the booster.

2. The trajectory is assessed, noting important parameters like propellant consump-

tion and dynamic pressure. It is found that the dynamic pressure on ascent has significant margin from the maximum allowable, while there is concern about the length of the vehicle for structural fatigue, especially for repeated landings.

3. A 10% increase in vehicle diameter whilst maintaining constant volume is proposed and the vehicle is simulated again with this updated configuration.

4. Upon assessment of the new trajectory, it is found that the ascent dynamic pressure remains within acceptable bounds. 4% more propellant is used across the ascent, but 15% less propellant is used in landing due to the lower centre of gravity and larger frontal area of the updated vehicle configuration.

5. The larger diameter is marked as an advisory design change.

Example 2: Mission feasibility of more affordable components

1. It is found by the propulsion team that a 50% cost reduction in the TVC subsystem could be achieved by using TVC actuators from an alternative supplier. However, these actuators have gimbal angle range that is 3 degrees less than that of the existing actuators.

2. It is unclear how a reduction in gimbal angle range would affect the ability of the vehicle to land successfully, especially for initial conditions near the limit of the expected range. The parameters of the alternative TVC actuators are adjusted within the simulator, and the landing module is run for a range of initial conditions.

3. It turns out that a negligible average performance hit across the full mission is taken by adopting the alternative actuators.

4. The alternative TVC actuators are marked as an advisory design change.

3

Simulator Detail Design

This chapter describes in detail the design assumptions and logical and mathematical implementation of the ascent, manoeuvre and landing modules which make up the whole-mission simulator for the RFA TWO booster.

3.1 Ascent Module

The ascent module of the simulator considers the dynamics of the fully-stacked launch vehicle during the initial phase of flight. The vehicle state is simulated across the ascent burn and uses defined vehicle and mission parameters to generate a classical gravity turn ascent profile. The booster stage separation gate is incorporated, after which the booster assumes ballistic dynamics. The ascent can be solved for a fixed staging velocity or altitude, or the maximum staging velocity irrespective of altitude.

3.1.1 Reference Frame

The ascent dynamics are modelled in an Earth-centred, Earth-fixed (ECEF) frame of reference as depicted in Figure 3.1, with the rotation of the Earth incorporated in the dynamics.

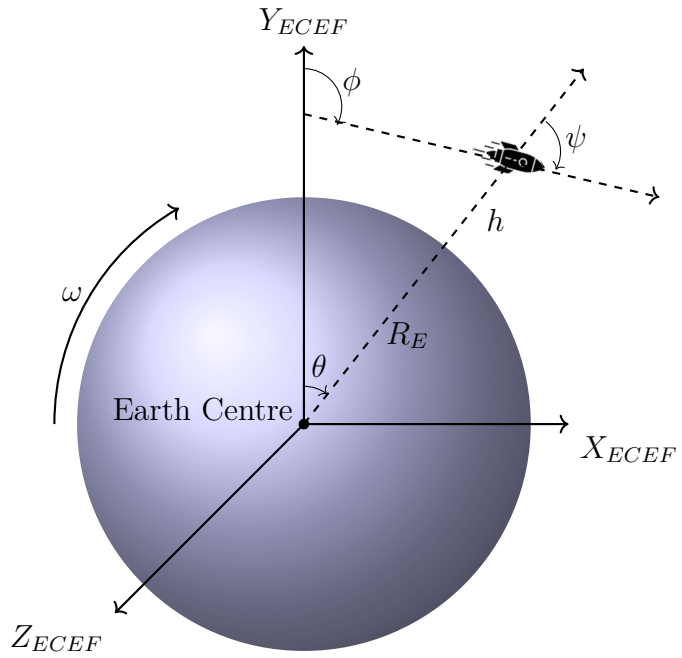

Figure 3.1: Earth-centred, Earth-fixed (ECEF) reference frame. R_E is the Earth's radius, h is the vehicle height above the Earth's surface, θ is the elevation angle, ψ is the flight path angle, ϕ is the azimuth angle and ω is the Earth's angular rotation.

3.1.2 Launch Site Considerations

RFA TWO is intended to [redacted] launch site (see Objective 08, Table 1.5). At [redacted]° latitude, the primary advantage of this location is its [redacted] which [redacted] Figure 3.2 shows the location of [redacted] within [redacted], where the [redacted] is evident.

Figure 3.2: Map of [redacted] annotated with coordinate grid and [redacted]

Within the ascent module of the simulator it is possible to define any launch site coordinates, with the resulting centrifugal and Coriolis accelerations appropriately captured in the dynamic model. For the purposes of the analyses and examples in this document, an equatorial orbit and launch site is assumed for ease of comprehension in two-dimensions. This approach is recommended as the default for iterative assessment of different vehicle configurations, as it provides a standard baseline from which to compare performance and eliminates the need to process output data in three dimensions.

3.1.3 Atmospheric Model

To accurately simulate aerodynamic forces during ascent, the NRLMSISE-00 atmospheric model[9] is accessed. Developed by the US Naval Research Laboratory, this model provides atmospheric properties such as air density and temperature as functions of altitude, latitude, longitude, time, and space weather conditions.

In the simulator, conditions are pre-computed based on atmospheric and space weather files fetched for a defined day of launch. Fixed latitude, longitude and time of the launch site are used - a reduction which reduces computational load and introduces negligible error since the vehicle travels [redacted] km downrange, at most.

3.1.4 Aerodynamic Drag Coefficients

Given that the simulator is intended for rapid, iterative assessment of various vehicle configurations, it is not recommended to conduct time-consuming computational fluid dynamics (CFD) simulations or wind tunnel testing to generate aerodynamic data for each vehicle configuration. Instead, the RASAero II software[10] can be utilised to generate aerodynamic drag coefficients over a range of Mach numbers, Reynolds numbers, and angles of attack. Similar in function to the US Air Force Missile DATCOM[11], RASAero II combines empirical data and theoretical models to provide reliable aerodynamic characteristics for the ascent phase.

Using the RASAero II tool, an aerodynamics database can be generated for use in the ascent module. In the ascent dynamics calculations, drag coefficients are accessed from the database based on the current altitude and velocity in the ECEF frame via the following function:

$$T = \texttt{atmosphereModel}(h) \tag{3.1}$$

$$a = \sqrt{\gamma R T} \tag{3.2}$$

$$Mach = \frac{v}{a} \tag{3.3}$$

$$C_{d,Mach} = \texttt{aero\_database}(Mach) \tag{3.4}$$

where T is the local air temperature, a is the local speed of sound, $\gamma = C_p/C_v \approx 1.401$

is the ratio of specific heats for air, $R \approx 286$ J/kg·K is the specific gas constant for air, v is the vehicle velocity magnitude, and $C_{d,Mach}$ is the Mach-dependent aerodynamic drag coefficient of the vehicle.

Since this method does not account for the decrease in atmospheric density with altitude, an exponential decay function is applied to the drag coefficient:

$$C_d(h) = C_{d,Mach} \cdot e^{-kh} \tag{3.5}$$

where k is a decay constant, calibrated based on an exoatmospheric "space threshold" altitude of 91.4 kilometres.

3.1.5 Ascent Forces

The model accounts for all major forces acting on the vehicle and includes provisions for Earth rotation and modulation of thrust for adherence to dynamic pressure constraints.

The acceleration due to gravity varies with altitude and is defined as:

$$g(h) = \frac{g_0}{\left(1 + \frac{h}{R_E}\right)^2} \tag{3.6}$$

where $g_0 \approx 9.807$ m/s^2 is the standard gravitational acceleration at sea level.

The centrifugal force that arises due to the non-inertial nature of the rotating ECEF frame augments the effective acceleration experienced by the vehicle. For an equatorial orbit [redacted], the centrifugal acceleration is given by:

$$a_{centrifugal} = \omega_{Earth}^2 \left(R_E + h\right) \tag{3.7}$$

where $\omega_{Earth} \approx 7.29 \times 10^{-5}$ rad/s represents the Earth's angular rotation rate. As a result of this force, the effective gravity experienced by the vehicle becomes:

$$g_{eff} = g(h) - a_{centrifugal} \tag{3.8}$$

At full power, the nominal propellant mass flow rate during the ascent burn is:

$$\dot{m}_{\text{nominal}} = -\frac{m_{\text{propellant}}}{t_{\text{burn}}} \tag{3.9}$$

However, to ensure that the dynamic pressure q remains below an allowable maximum q_{max}, the mass flow rate can be modulated:

$$q = \frac{1}{2}\rho v^2 \tag{3.10}$$

$$\dot{m}(q) = \dot{m}_{\text{nominal}} \cdot \min\left(1, \frac{q_{\max}}{q(h)}\right) \tag{3.11}$$

where ρ and v are the local air density velocity, respectively. This modulation effectively reduces the thrust when the dynamic pressure approaches or exceeds $q_{\max}$. The resulting thrust produced by the engines is therefore:

$$T = -\dot{m}(q) \cdot v_e \tag{3.12}$$

where v_e is the effective exhaust velocity, while the mass as a function of time across the ascent is defined by:

$$m(t) = m_0 + \int_0^t \dot{m}(q), dt \tag{3.13}$$

The drag force acting on the vehicle is given by:

$$D = \frac{1}{2}\rho v^2 A_{\text{ref}} C_d \tag{3.14}$$

where A_{ref} is a reference area which represents the frontal projection area of the vehicle including [redacted].

3.1.6 Equations of Motion

The translational and rotational dynamics are governed by the derivatives of velocity v, altitude h, elevation angle θ, flight path angle ψ, and downrange distance x. An equatorial orbit [redacted] is assumed so that Coriolis forces are not present in the equations of motion.

Three distinct periods are defined within the ascent, each with specific dynamics and control laws.

Vertical period

The vertical period is active from lift-off until an altitude h_{turn} at which the gravity turn pitch-over is initiated. The value of h_{turn} is determined by an optimisation loop within the simulation logic and depends on the particular staging altitude, staging velocity, or maximum staging velocity that has been chosen for the ascent module to solve for.

During the vertical period, the vehicle ascends with a very small flight path angle which provides no more than enough deviation from the vertical to clear the launch tower. The dynamics for the vertical period are as follows:

$$\dot{m} = \dot{m}_{\text{nominal}} \cdot \min\left(1, \frac{q_{\max}}{q(h)}\right) \tag{3.15}$$

$$\dot{v} = \frac{T}{m} - \frac{D}{m} - g_{eff}\cos(\psi_0) \tag{3.16}$$

$$\dot{h} = v \tag{3.17}$$

$$\dot{\theta} = 0 \tag{3.18}$$

$$\dot{\psi} = 0 \tag{3.19}$$

$$\dot{x} = 0 \tag{3.20}$$

Gravity turn period

When h_{turn} is reached, the dynamics change to facilitate a natural gravity turn where the flight path angle gradually increases from the small initial value which seeds the dynamics:

$$\dot{m} = \dot{m}_{\text{nominal}} \cdot \min\left(1, \frac{q_{\max}}{q(h)}\right) \tag{3.21}$$

$$\dot{v} = \frac{T}{m} - \frac{D}{m} - g_{eff}\cos(\psi) \tag{3.22}$$

$$\dot{h} = v\cos(\psi) \tag{3.23}$$

$$\dot{\theta} = \frac{v\sin(\psi)}{R_E + h} \tag{3.24}$$

$$\dot{\psi} = \frac{g_{eff}\sin(\psi)}{v} - \dot{\theta} \tag{3.25}$$

$$\dot{x} = (R_E + h)\dot{\theta} \tag{3.26}$$

Ballistic coast period

The coast period begins when the booster has expended all propellant allocated for the ascent. During this period, thrust is zero and the rocket coasts in a ballistic fashion under inertia and gravitational forces, with the flight path angle evolving naturally. The equations of motion are defined as:

$$\dot{m} = 0 \tag{3.27}$$

$$\dot{v} = -\frac{D}{m} - g_{eff}\cos(\psi) \tag{3.28}$$

$$\dot{h} = v\cos(\psi) \tag{3.29}$$

$$\dot{\theta} = \frac{v\sin(\psi)}{R_E + h} \tag{3.30}$$

$$\dot{\psi} = \frac{g_{eff}\sin(\psi)}{v} - \dot{\theta} \tag{3.31}$$

$$\dot{x} = (R_E + h)\dot{\theta} \tag{3.32}$$

A fifth-order Runge-Kutta (RK45) numerical integration method is employed to propagate the dynamics and produce an ascent trajectory.

3.1.7 Example Ascent Trajectories

Examples of trajectories generated by the ascent module for a given RFA TWO vehicle configuration are provided. The vehicle configuration used in both examples is identical - only the booster staging conditions for the ascent module to solve for are varied. Note that these are ballistic trajectories and do not include any manoeuvre or landing phases.

Specific staging altitude

For the trajectory shown in 3.3, the ascent module was set to solve for a staging altitude of [redacted] km. The simulator determined that the optimal value of h_{turn} in this case was [redacted] m with a staging velocity of around [redacted] m/s.

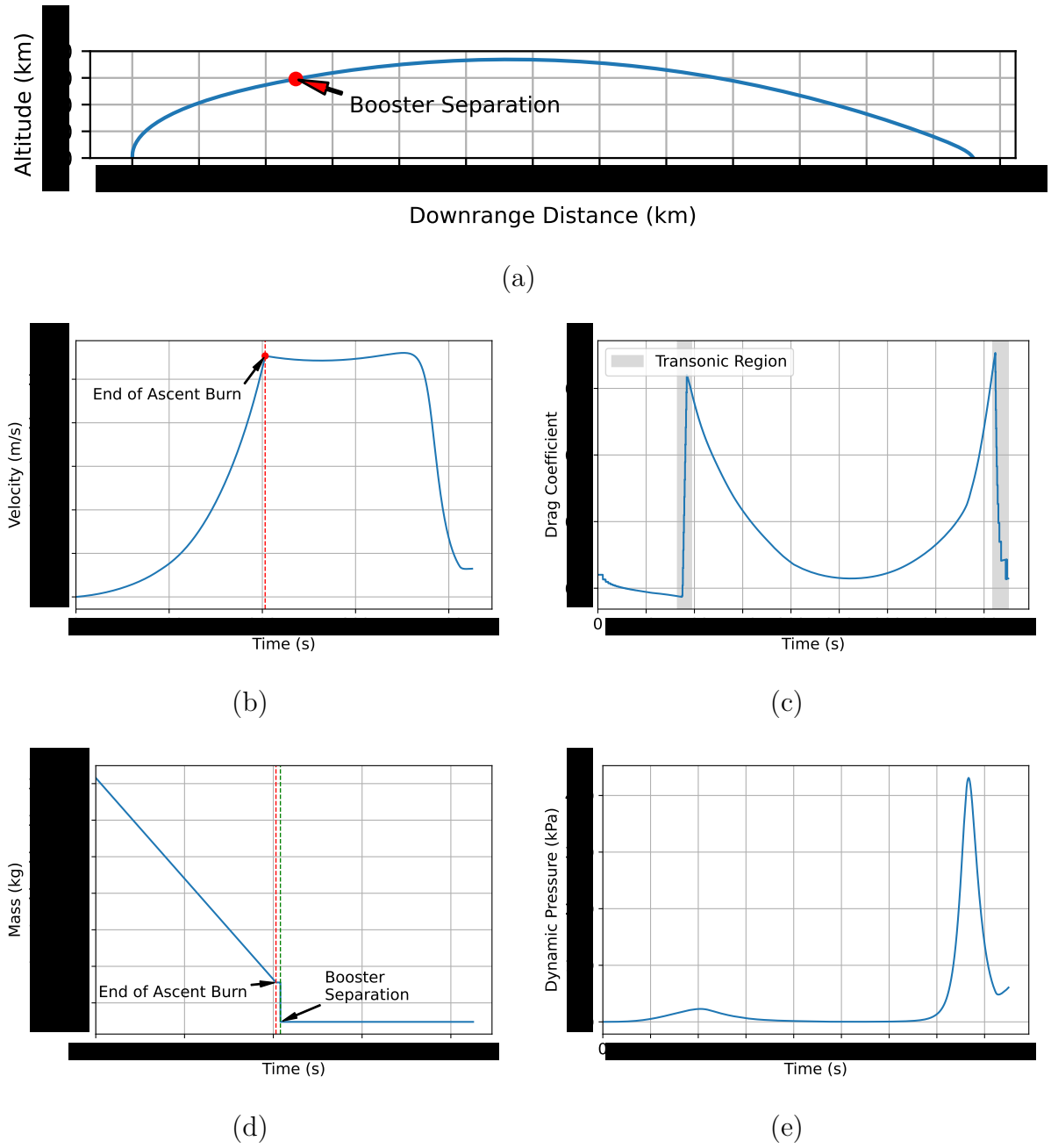

Figure 3.3: Example ballistic booster trajectory for a staging altitude of [redacted] km for a given vehicle configuration

Maximum staging velocity

For the trajectory shown in Figure 3.4, the ascent module was set to solve for a maximum staging velocity, irrespective of altitude. The staging velocity achieved was around [redacted] m/s at an altitude of approximately [redacted] km. The corresponding value of h_{turn} was [redacted] m.

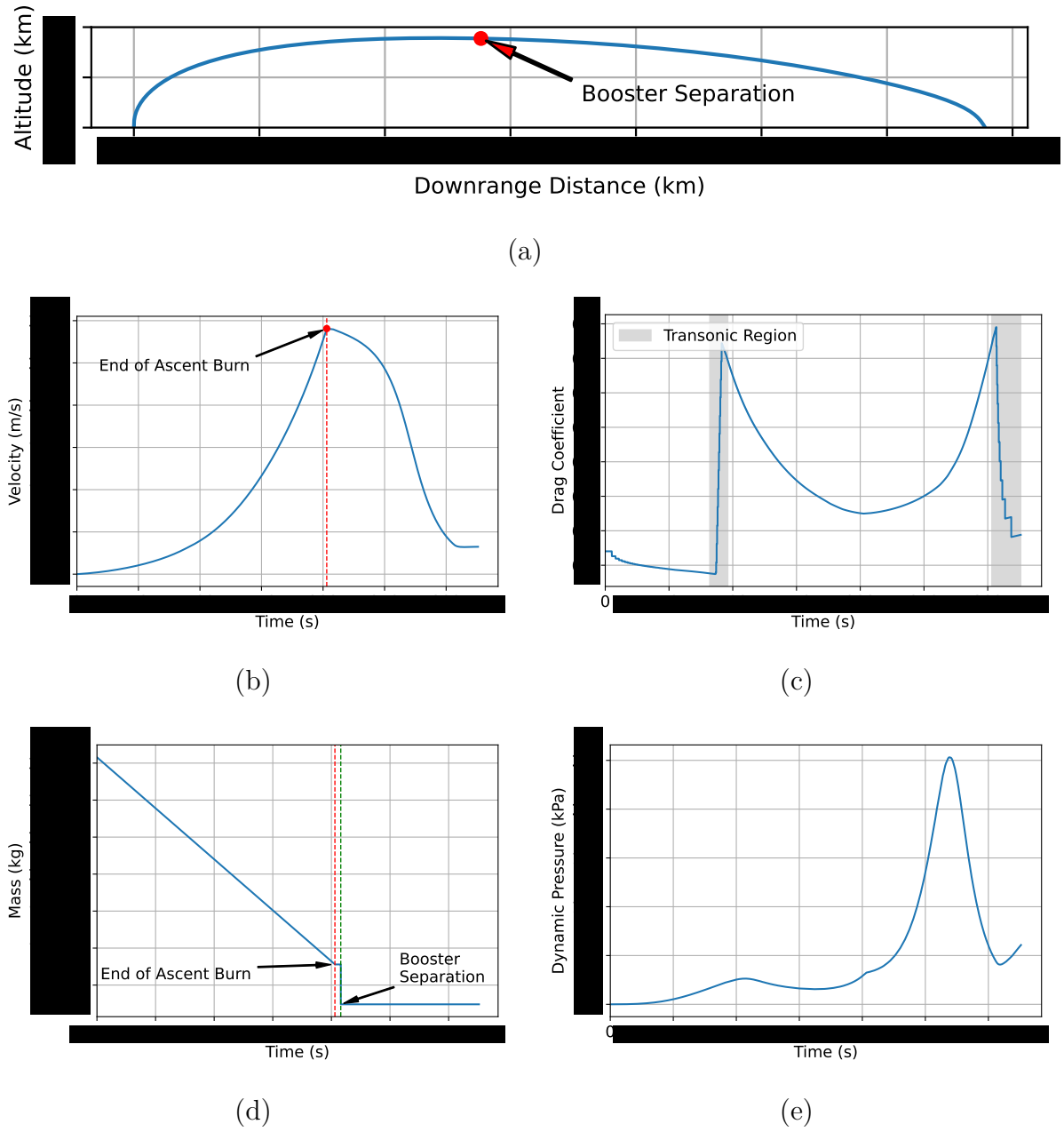

Figure 3.4: Example RFA TWO ballistic booster trajectory solved for the maximum staging velocity for a given vehicle configuration

3.2 Manoeuvre Module

The purpose of the manoeuvre module of the simulator is to gain an understanding of the in-space manoeuvrability of the booster. With reference again to the downrange landing ConOps (Figure 2.1), it is clear that a key phase of the mission profile is the re-orientation of the booster such that the thrust vector is aligned favourably for landing.

Such manoeuvres take place at altitudes where air density is too low for aerodynamic control surfaces to work effectively. It is for this reason that [redacted]

[redacted] to control the booster orientation. The manoeuvre module takes the inertial properties of the booster into account so that the rigid body dynamics required to model the [redacted] are appropriately captured.

Although the manoeuvre dynamics only affect the booster orientation or *attitude*, it is important to highlight that the the vehicle, of course, is still in ballistic translational motion. As such, translational dynamics still act passively on the booster during the manoeuvre phase. The manoeuvre module assumes that the [redacted] are perfectly aligned so that they do not impart translational impulses and that atmospheric drag, lift, and aerodynamic torques are assumed to be negligible due to the high altitude at which the [redacted] manoeuvres are performed. With these assumptions, the translational and rotational dynamics are effectively decoupled and can be modelled independently to a reasonable approximation for analysis purposes.

3.2.1 Reference Frame and Model Geometry

The manoeuvre module uses the same ECEF frame of reference as the ascent module, shown in Figure 3.1. The [redacted] dynamic model abstracts away the specific details of the [redacted] subsystem, considering only its basic geometry and performance characteristics. The [redacted] is modelled as [redacted] located at distance $x_{\text{[redacted]},\,\text{i}}$ from the centre of mass (CoM) of the booster and [redacted] normal to the longitudinal axis, producing a torque which rotates the vehicle transversely. The moment arms $l_{\text{[redacted]},\,\text{i}}$ for [redacted] torque generation are therefore:

$$l_{\text{[redacted]},\,\text{i}} = x_{\text{[redacted]},\,\text{i}} - x_{\text{CoM}} \tag{3.33}$$

To model more complex [redacted] configurations, the sum of the individual components of thrust acting in the plane of rotation that are provided by each thruster can be found trigonometrically.

Figure 3.5 shows the [redacted] dynamic model geometry, where it is evident that the ECEF flight path angle ψ continues to follow ballistic translational dynamics while the attitude angle α describes a pure rotation of the booster about its centre of mass.

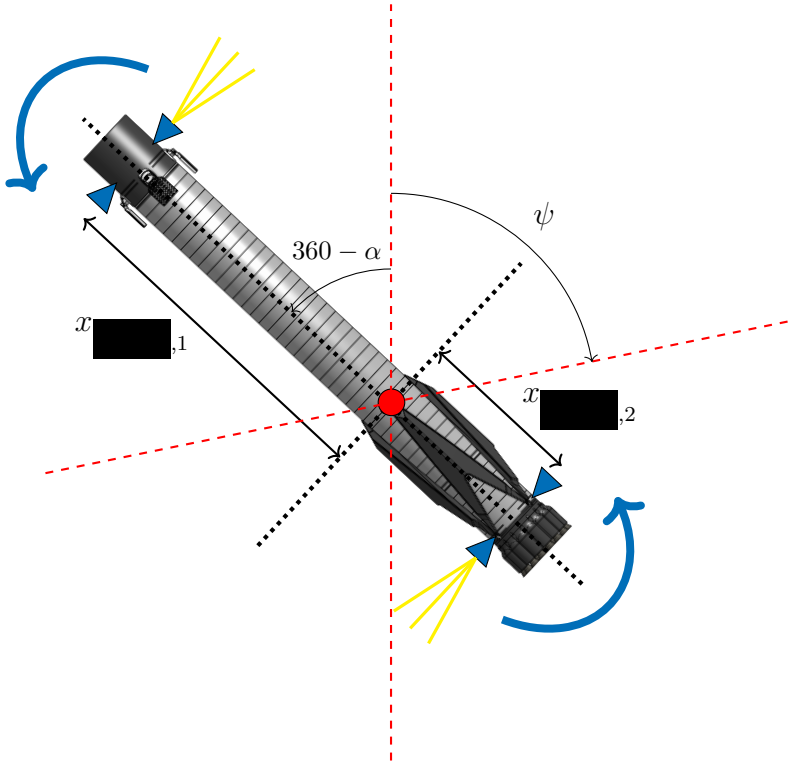

Figure 3.5: [redacted] model geometry, where ψ is the ECEF flight path angle, α is the booster attitude angle, and x [redacted],1 and x [redacted],2 are the longitudinal distances between the respective [redacted] and the booster CoM

3.2.2 Booster Inertial Properties

Within the simulator, the manoeuvre module is initiated after a defined booster separation buffer time, at which point the booster contains only the required propellant, plus any margin, to complete the engine burns for retro-propulsive landing. With an estimate of this landing propellant mass, and therefore an estimate of the total vehicle mass during the manoeuvre phase, it is possible to approximate the CoM and transverse moment of inertia (MoI) of the booster, parameters which are necessary for simulating and characterising the [redacted].

CoM and MoI values can be determined with varying degrees of accuracy. If a full-featured mass model of the vehicle is available, standard computer-aided design tools will provide the best estimate of inertial parameters. However, for [redacted], alternative approaches must be taken.

One approach involves using approximations and reasonable assumptions about the booster geometry and mass distribution by dividing it into its major elements as in Figure 3.6.

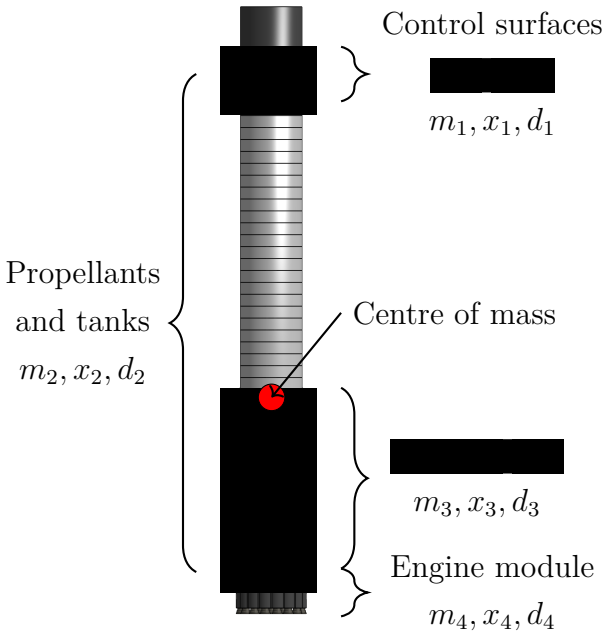

Figure 3.6: Example distribution of major RFA TWO booster elements i, each with mass m_i, mean distance from base x_i and mean distance from booster CoM d_i

The following assumptions are made:

- The booster is approximated as a cylindrical structure with non-uniform mass distribution along the longitudinal axis.
- Only major elements affecting inertial properties are considered.
- Elements are symmetrically distributed around the longitudinal axis.
- The transverse axis is perpendicular to the longitudinal axis and passes through the CoM.

The booster CoM can be estimated by considering the mass distribution of the booster's significant elements or components along the longitudinal axis:

$$x_{\text{CoM}} = \frac{\sum_i m_i x_i}{\sum_i m_i}, \quad \sum_i m_i \approx m_{\text{expected}} \tag{3.34}$$

where m_i is the mass of element i, x_i is the longitudinal position of element i's CoM relative to a reference point (e.g., the base of the booster), and m_{expected} is the expected mass of the booster at the point of manoeuvre, where the booster contains only the propellant required for retro-propulsive landing.

The total transverse moment of inertia I_{total} about the booster CoM is determined

using the parallel axis theorem:

$$I_{\text{total}} = \sum_i \left(I_i + m_i d_i^2 \right) \tag{3.35}$$

where I_i is the transverse moment of inertia of element i about its own CoM, and d_i is the distance from the booster's CoM to element i's CoM.

Some general moment of inertia formulae for various approximated element geometries with radii R and lengths L that can be applied are:

- Thin-walled shells (e.g., propellant tanks):

$$I_i = m_i \left(R_{\text{mean}}^2 + \frac{L^2}{12} \right) \tag{3.36}$$

- Solid cylinders (e.g., bulk propellant):

$$I_i = \frac{1}{12} m_i \left(3R^2 + L^2 \right) \tag{3.37}$$

- Point masses (e.g., engines):

$$I_i = 0 \tag{3.38}$$

  The contribution of point masses to the total moment of inertia is through the $m_i d_i^2$ term in Equation 3.35.

3.2.3 Manoeuvre Dynamics and Control

When the manoeuvre commences, the booster attitude angle is allowed to decouple from the flight path angle. At this point, a proportional, integral, derivative (PID) controller is applied to determine the total [redacted] command $T_{[redacted]}$ at each integration step k required to reduce the error between the booster attitude and the target attitude, α_{target}. The PID errors are defined as:

$$e_p[k] = \alpha[k] - \alpha_{target} \tag{3.39}$$

$$e_i[k] = e_i[k-1] + e_p[k]\Delta t \tag{3.40}$$

$$e_d[k] = \frac{e_p[k] - e_p[k-1]}{\Delta t} \tag{3.41}$$

where e_p, e_i and e_d are the proportional, integral and derivative errors, respectively, and Δt is the time between integration steps k and $k-1$. The resulting total [redacted]

command computed by the PID controller is:

$$T_{[redacted]} = K_p e_p + K_i e_i + K_d e_d \quad \text{subject to} \quad |T_{[redacted]}| \leq 2 \cdot T_{[redacted]} \tag{3.42}$$

where K_p, K_i and K_d are the proportional, integral and derivative gains, respectively, and $T_{[redacted],\,\max}$ is the maximum thrust of [redacted]. The torque $\tau_{[redacted]}$ applied is given by:

$$\tau_{[redacted]} = \frac{T_{[redacted]} \cdot l_{[redacted],1}}{2} + \frac{T_{[redacted]} \cdot l_{[redacted],2}}{2} \tag{3.43}$$

with the resulting angular acceleration $\ddot{\alpha}$:

$$\ddot{\alpha} = \frac{\tau_{[redacted]}}{I_{\text{total}}} \tag{3.44}$$

and angular velocity $\dot{\alpha}$:

$$\dot{\alpha} = \frac{d\ddot{\alpha}}{\Delta t} \tag{3.45}$$

While the manoeuvre progresses, the translational motion of the vehicle continues to propagate via the ballistic coast dynamics such that:

$$\dot{m} = 0 \tag{3.46}$$

$$\dot{v} = -\frac{D}{m} - g_{eff}\cos(\psi) \tag{3.47}$$

$$\dot{h} = v\cos(\psi) \tag{3.48}$$

$$\dot{\theta} = \frac{v\sin(\psi)}{R_E + h} \tag{3.49}$$

$$\dot{\psi} = \frac{g_{eff}\sin(\psi)}{v} - \dot{\theta} \tag{3.50}$$

$$\dot{x} = (R_E + h)\dot{\theta} \tag{3.51}$$

The manoeuvre terminates after a maximum manoeuvre time gate $t_{[redacted],end}$, at which point the attitude rate of the booster is re-coupled with the flight path angle.

3.2.4 Example Manoeuvre Profiles

The performance of the [redacted] can be assessed by observing the time taken for the booster to arrive at the desired attitude and the control effort (thrust) required. Knowledge of the latter could be used to determine the [redacted] required for a given vehicle configuration.

Initial conditions and inertial properties of the booster are identical for each of the

following examples, as is the [redacted] time gate $t_{[redacted],end}$.

Target attitude: 275°, maximum thrust [redacted]: [redacted] N

Figure 3.7 shows an example manoeuvre trajectory for a desired attitude angle α_{target} of 275°and a maximum combined [redacted] of [redacted] N [redacted]. The attitude and attitude rate reach a steady state before the [redacted] gate.

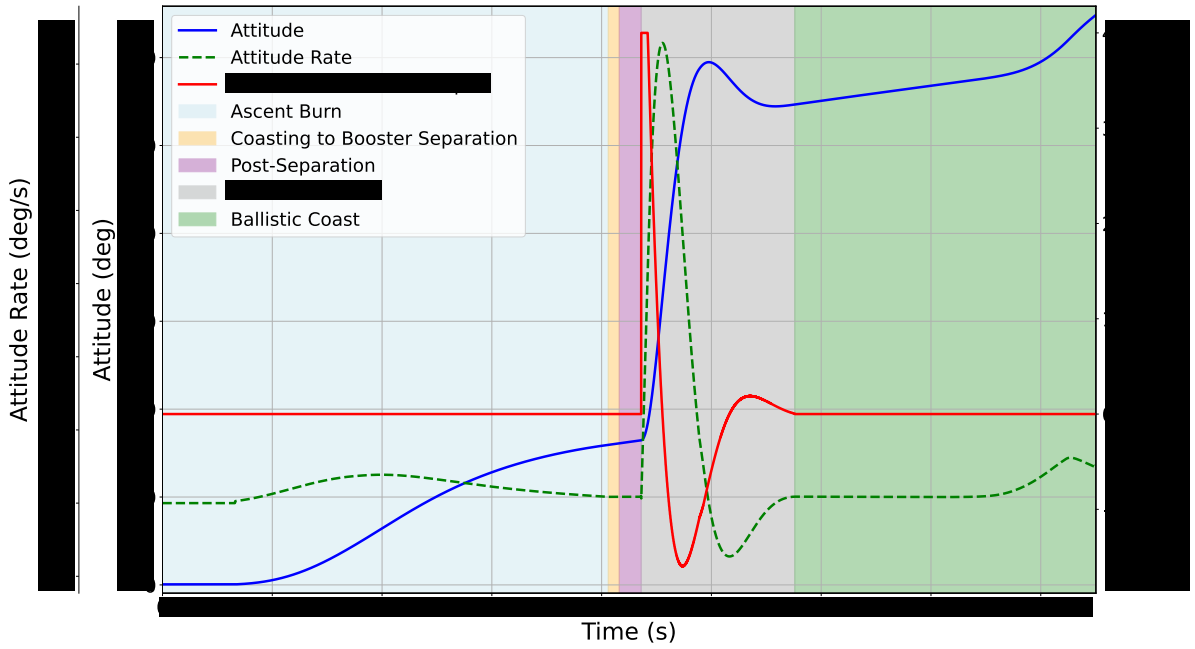

Figure 3.7: Example manoeuvre profile and [redacted] for $\alpha_{target} = 275°$, $T_{[redacted],max} = [redacted]N$

Target attitude: 0°, maximum [redacted]: [redacted] N

Figure 3.8 shows an example manoeuvre trajectory for a desired attitude angle α_{target} of 0°and a maximum [redacted] of [redacted] N [redacted]. In this case, it is clear to see that the attitude and attitude rate do not reach a steady state before the manoeuvre termination gate. This could be an indication that a [redacted] configuration may not be suitable for the booster configuration in question without an increase in allotted manoeuvre time.

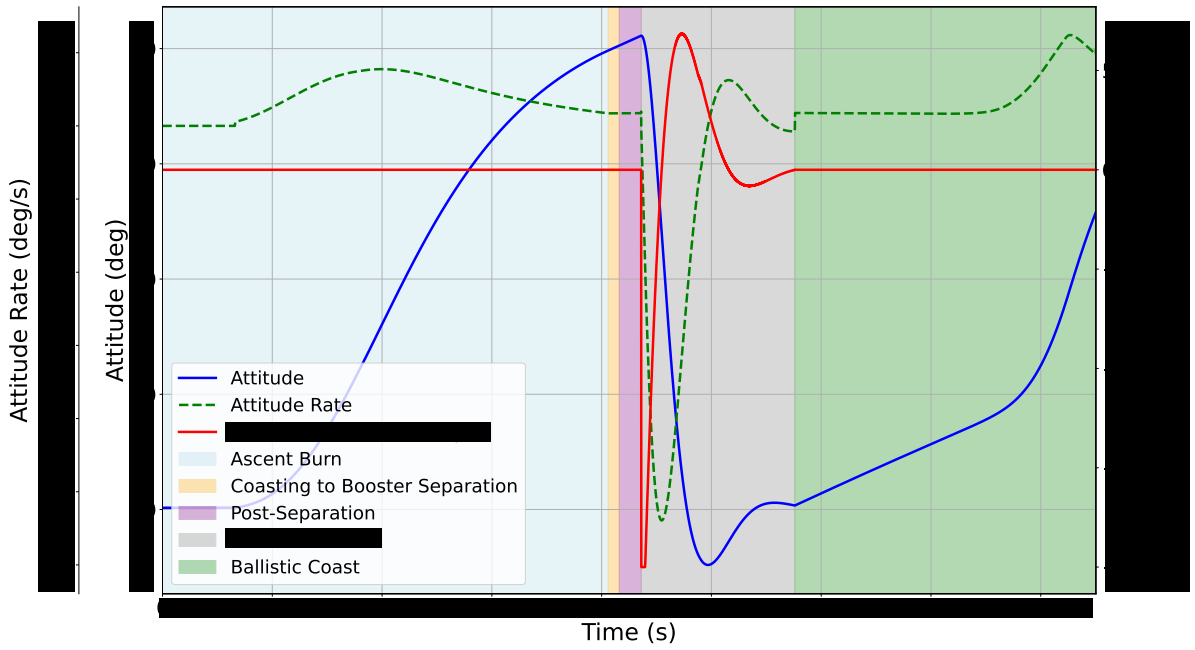

Figure 3.8: Example manoeuvre profile and [redacted] application for $\alpha_{target} = 0°$, $T_{[redacted],max} = [redacted]N$

3.3 Landing Module

The landing module of the simulator represents the main contribution of this project, employing state-of-the-art, robust convex programming techniques to generate propellant-optimal retro-propulsive booster landing trajectories.

The landing algorithm works on the principle of convexification, which involves the reformulation of a non-convex problem into a convex one by applying various mathematical and logical re-structuring techniques. The specific techniques used, namely lossless convexification and successive convexification, were first applied to the problem of retro-propulsive landing by aerospace guidance, navigation and control (GNC) engineering researchers Behçet Açıkmeşe (University of Washington), Lars Blackmore (SpaceX) and colleagues. Their work proved that non-convex spacecraft landing trajectory optimisation problems can be reformulated in convex ways through carefully-chosen approximations and linearisations[12]. Convexification of the problem allows computationally-tractable solutions to be obtained that are guaranteed to be globally optimal within the confines of the convexified solution space and, by extension, within the non-convex solution space due to the lossless nature of the manipulations applied.

The particular implementation in this project uses lossless and successive convexification methods and disciplined convex programming (DCP) techniques to formulate the landing problem such that it can be solved using open-source libraries and solvers such as those packaged within the CVXPY Python-embedded modelling language[13], presenting

a significant benefit for RFA.

3.3.1 Problem Outline

The problem of propellant-optimal retro-propulsive landing of an orbital rocket booster is challenging due to the high dimensionality, stringent constraints and complex dynamics, as well as the necessity for robustness to a range of boundary conditions to suit various mission profiles. The aim is to produce a trajectory that guides the booster to a designated landing location while minimising propellant consumption and ensuring that the trajectory:

- Is feasible and adheres to physical laws
- Respects defined boundary conditions related to the vehicle performance, configuration and physical limitations
- Meets precise terminal conditions - the vehicle must have near-zero velocity, an upright orientation and minimal lateral position error at the end of its descent
- Is robust to uncertainties and disturbances like engine or actuator failure and wind shear

Possible approaches to solve this kind of problem include model-predictive control (MPC), reinforcement learning (RL), and convex/non-convex optimisation.

3.3.2 Convex and Non-Convex Problems

A convex problem is one where any local minimum in the feasible solution set defined by the objective function and constraints is also a global minimum. The general form of a convex optimisation problem is:

$$\begin{aligned} \text{minimise} \quad & f_0(x) && (3.52)\\ \text{subject to} \quad & f_i(x) \leq 0, \quad i = 1, \ldots, m && (3.53)\\ & a_i^\top x = b_i, \quad i = 1, \ldots, p && (3.54) \end{aligned}$$

where $x \in \mathbb{R}^n$ is an optimisation variable, $f_0 : \mathbb{R}^n \to \mathbb{R}$ is the convex objective function and $f_i : \mathbb{R}^n \to \mathbb{R}$ are convex inequality constraints. The equality constraints $a_i^\top x = b_i$ are affine.

In contrast, a non-convex optimisation problem is one where the objective function or the feasible region is non-convex. In this case, the feasible solution space may have multiple local minima, regions where the second derivative is negative, or disjointed

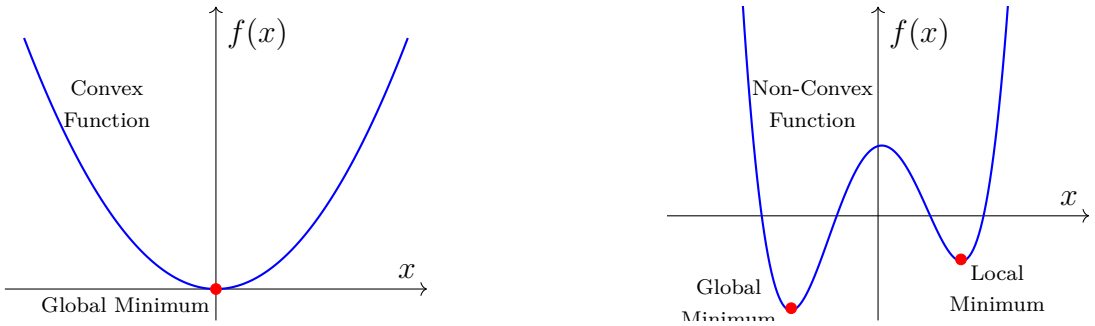

(a) Convex Problem (b) Non-Convex Problem

Figure 3.9: Comparison between simple convex and non-convex optimisation problems

regions or "holes". Figure 3.9 shows a comparison between the topologies of simple convex and non-convex problems.

Numerical approaches for solving all classes of optimisation problem are typically gradient-based, meaning that they seek to find a point in the solution space where the derivative is equal to zero, indicating a minimum. Solver codes may therefore become "stuck" in suboptimal solutions when dealing with multiple local optima in non-convex solution spaces, while more advanced interior-point method (IPM) solvers which traverse the interior of the solution space have difficulty dealing with non-continuity introduced by disjointed regions in non-convex sets.

Machine learning-type approaches, genetic families of algorithms and other non-traditional solvers are often capable of finding near-optimal solutions within non-convex sets, though these methods do not systematically leverage gradients or second-order information and often rely on repeated random sampling processes that scale poorly with problem complexity. This can result in high computational cost and uncertain solution quality. Machine learning models, if trained, require extensive offline training on large datasets that must be representative of all flight conditions - introducing challenges in coverage, generalisation, and verification.

Thus, in practice, it is advantageous to formulate optimisation problems in a convex way. The geometry of a convex solution space guarantees, mathematically, that the local minimum is also the global minimum. However, for real-world engineering problems, the limited scope of convex problem formulations rarely captures the full complexity of the case. The non-linear, coupled dynamics and constraints such as those of the retro-propulsive landing problem produce highly non-convex formulations in their pure, untreated forms.

In many cases, certain mathematical and algorithmic "convexification" techniques can be applied to complex non-convex problem formulations in order to arrive at computationally-tractable versions. Such techniques include reformulating constraints, changing variables, or applying lossless relaxations that approximate the original problem. Through these methods, it becomes possible to leverage convex optimisation solvers that can efficiently

compute a global solution with provable optimality guarantees.

3.3.3 Reference Frame

The landing is not defined in the ECEF reference frame as it is more relevant and convenient to define, describe and model the landing with respect to the landing site than to the centre of the Earth. When the vehicle is close to the target location, the curvature and rotation of the Earth and large-scale geodetic coordinates become less relevant. Instead, local topography dominates. A local Up-East-North (UEN) coordinate system is defined with the East-North plane in the region of the targeted landing site as shown in Figure 3.10.

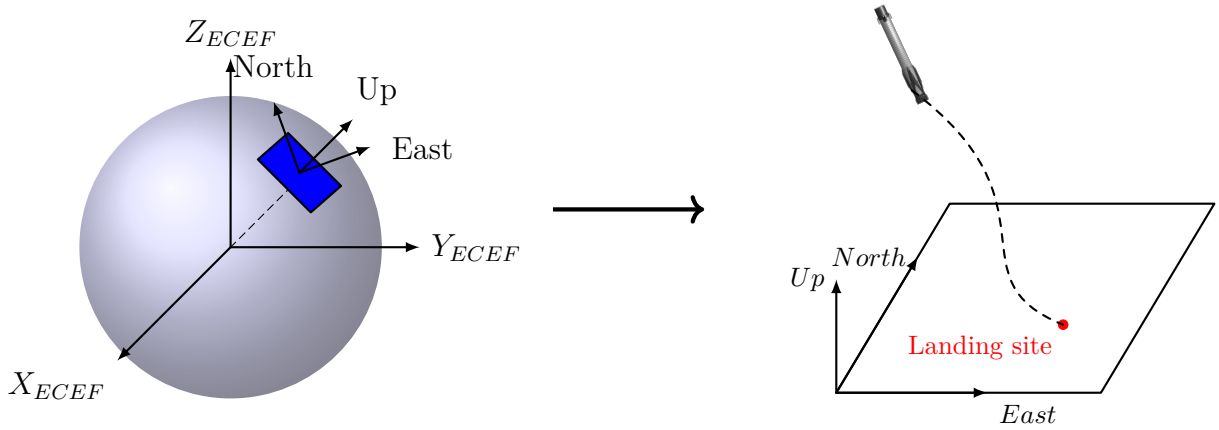

Figure 3.10: Local Up-East-North frame of reference for booster landing

3.3.4 Untreated Problem Formulation

The discrete-time objective function of the untreated landing problem is simply a maximisation of the final booster mass via constrained optimisation of the time of flight and thrust vector, with the final mass serving as a lossless proxy for total propellant consumption:

$$\underset{\Delta t, \mathbf{T}}{\text{maximise}} \quad m[k_f] \tag{3.55}$$

Constraints

A constraint is placed to ensure that feasibility can only be achieved with the mass at any point being greater than the booster inert mass:

$$m_{inert} \leq m[k] \tag{3.56}$$

A constraint on the vehicle position vector $\mathbf{r}$ is defined to ensure that the trajectory does not place the booster outside of an inverted cone centred on the desired landing site with

half-angle γ_{gs}:

$$||\mathbf{r}|| \cos(\gamma_{gs}) \leq \hat{\mathbf{e}}_u^\top \mathbf{r}[k] \tag{3.57}$$

Bounds are placed on the thrust vector:

$$0 \leq T_{min} \leq ||\mathbf{T}[\mathbf{k}]|| \leq T_{max} \tag{3.58}$$

The maximum tilt angle for the booster is defined as θ_{max}, and is constrained via the thrust vector with:

$$||\mathbf{T}[k]|| \cos(\theta_{max}) \leq \hat{\mathbf{e}}_u^\top \mathbf{T}[k] \tag{3.59}$$

Finally, the rate of change of thrust magnitude is bounded based on the throttling capabilities of the propulsion system:

$$\dot{T}_{min} \leq \frac{||\mathbf{T}[k+1]|| - ||\mathbf{T}[k]||}{\Delta t} \leq \dot{T}_{max} \tag{3.60}$$

Dynamics

The mass depletion dynamics are given by:

$$\alpha = \frac{1}{I_{sp} g_0} \tag{3.61}$$

$$\dot{m}_{bp} = \frac{P_{amb} A_{nozzle}}{I_{sp} g_0} \tag{3.62}$$

$$m[k+1] = m[k] - \left[\frac{\alpha}{2}\left(||\mathbf{T}[k]|| + ||\mathbf{T}[k+1]||\right) + \dot{m}_{bp}\right] \tag{3.63}$$

where α is a mass depletion factor, $\dot{m}_{bp}$ is the mass flow loss due to back-pressure, P_{amb} is the ambient pressure and A_{nozzle} is the combined nozzle exit area of the engines in use for the landing burn. The drag force is:

$$\mathbf{D}[k] = -\frac{1}{2}\rho S_D C_D ||\mathbf{v}[k]|| \mathbf{v}[k] \tag{3.64}$$

where S_D is the longitudinal projection area of the booster, including any peripheral hardware such as landing legs. Finally, the position, velocity and acceleration dynamics are given by:

$$\mathbf{r}[k+1] = \mathbf{r}[k] + \mathbf{v}[k]\Delta t + \frac{1}{3}\left(\mathbf{a}[k] + \frac{1}{2}\mathbf{a}[k+1]\right)\Delta t^2 \tag{3.65}$$

$$\mathbf{v}[k+1] = \mathbf{v}[k] + \frac{1}{2}\left(\mathbf{a}[k] + \mathbf{a}[k+1]\right)\Delta t \tag{3.66}$$

$$\mathbf{a}[k] = \frac{1}{m[k]}\left(\mathbf{T}[k] + \mathbf{D}[k]\right) + \mathbf{g} \tag{3.67}$$

3.3.5 Convexification of the Untreated Formulation

The untreated problem formulation as described in Section 3.3.4 is not readily solvable due to non-convexities related to the thrust constraints and the non-linear terms present in the dynamics. Each of these sources of non-convexity can be systematically convexified in order to arrive at a tractable problem.

Minimum thrust constraint

Classical rocket engines are not capable of throttling down to zero thrust magnitude. The [redacted] propulsion system of RFA TWO is expected to have a minimum thrust of around [redacted]% of the maximum, and its use of [redacted] limits the system to [redacted] burn. As such, the set of possible thrust vectors $\mathbf{T}(t)$ is non-convex since any two points in the feasible region cannot be connected without traversal over non-feasible space produced by the lower bound on the thrust magnitude, T_{min}:

$$0 \leq T_{min} \leq ||\mathbf{T}(t)|| \leq T_{max} \tag{3.68}$$

The non-convexity in the thrust constraint from the untreated problem forumlation (Equation 3.58is shown graphically in Figure 3.11(a). It turns out that this constraint

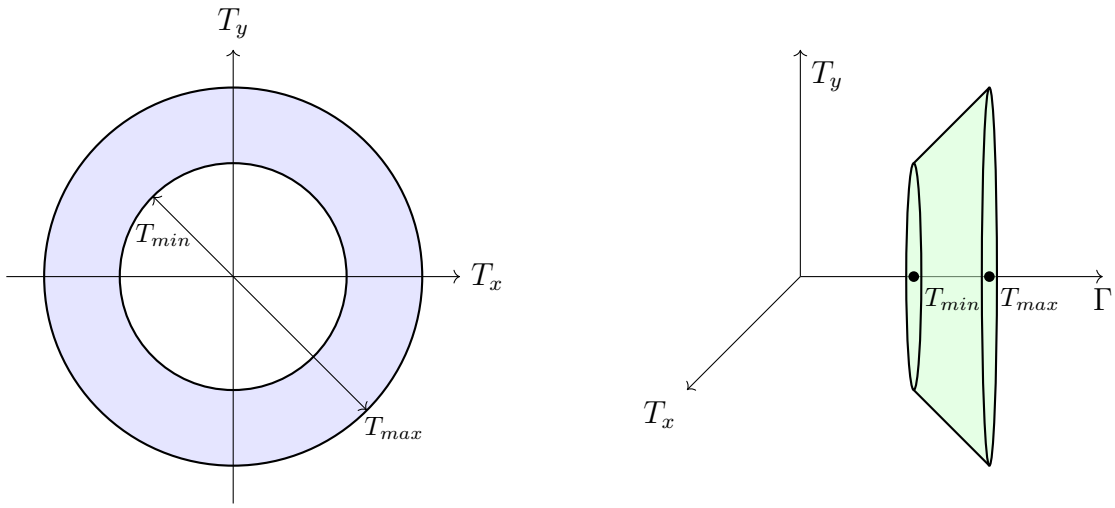

(a) Non-convex set of feasible thrust vectors $\mathbf{T}$

(b) Convexified set of feasible $(\mathbf{T}, \Gamma)$ pairs

Figure 3.11: Convexification of the minimum thrust constraint

can be "convexified" without loss of generality by introducing an auxiliary scalar variable Γ which represents the thrust magnitude only and is bound by inequality constraints:

$$||\mathbf{T}(t)|| \leq \Gamma(t) \tag{3.69}$$

$$0 \leq T_{min} \leq \Gamma(t) \leq T_{max} \tag{3.70}$$

This modification decouples the thrust magnitude constraint from the direction of $\mathbf{T}(t)$, allowing the magnitude and direction to be handled separately within the optimisation problem. Thus, the new set of feasible $(\mathbf{T}, \Gamma)$ pairs forms a convex set as shown in Figure 3.11(b). This process is known as *lossless convexification* - lossless because any optimal solution in the convexified set is also an optimal solution to the original problem.

Non-linear terms

The untreated problem formulation contains several non-linear terms. These terms are associated with vehicle mass depletion dynamics, aerodynamics, and free final landing time. Non-linearity gives rise to non-convexity due to the presence of products, ratios, or non-linear functions of the decision variables.

Including the final time t_f as a free decision variable means that the Δt terms in the dynamics are multiplied with other decision variables. The presence of such products (e.g. $\mathbf{v}[k]\Delta t$ and $\mathbf{a}[k](\Delta t)^2$) introduces bilinear and and quadratic terms, leading to a non-convex solution space.

In the drag force dynamics from the untreated problem formulation (Equation 3.64), a quadratic dependence arises because $\mathbf{D}[k]$ involves the magnitude of velocity $||\mathbf{v}k||$. The velocity vector $\mathbf{v}(t)$ is multiplied by this magnitude such that:

$$\mathbf{D}(t) \propto ||\mathbf{v}(t)||\mathbf{v}(t) \tag{3.71}$$

Substituting $\mathbf{v}(t) = ||\mathbf{v}(t)||\hat{\mathbf{v}}(t)$, the drag magnitude becomes proportional to $||\mathbf{v}(t)||^2$, a quadratic function that introduces non-linearity - and by extension, non-convexity - into the drag force calculation.

With $\mathbf{D}[k]$ being a non-linear function of $\mathbf{v}[k]$, and with $\mathbf{a}[k]$ depending on $\mathbf{D}[k]$, the acceleration dynamics also become non-linear and non-convex.

The inclusion of the mass in the acceleration dynamics is the final source of non-linearity. The acceleration $\mathbf{a}[k]$ is given by:

$$\mathbf{a}[k] = \frac{1}{m[k]} \left(\mathbf{T}[k] + \mathbf{D}[k]\right) + \mathbf{g} \tag{3.72}$$

The mass $m[k]$ appears in the denominator and varies over time due to propellant consumption. As the mass decreases, it affects the acceleration non-linearly. The inverse of an optimisation variable, $\frac{1}{m[k]}$ in this case, is a non-linear function which introduces non-convexity into the dynamics.

The non-convexity associated with these non-linear functions can be addressed using the technique of *successive convexification*. This method transforms the untreated

optimisation problem into a series of convex sub-problems that can be solved iteratively.

An initial guess of the trajectory is first defined by assuming linear mass and speed profiles and estimating a time of flight based on the distance between the vehicle and the landing site at the beginning of the landing phase. The resulting trajectory is taken as a basis around which to linearise, with the process of linearisation around previous trajectories repeating until convergence is reached.

Initialisation

The linear mass and speed profiles $\mu[k]$ and $s[k]$ defined for the initial trajectory estimate are calculated as:

$$\mu[k] = \left(\frac{k_n - k}{k_n}\right) m_0 + \left(\frac{k}{k_n}\right) m_{inert} \tag{3.73}$$

$$s[k] = \left(\frac{k_n - k}{k_n}\right) ||\mathbf{v}_0|| + \left(\frac{k}{k_n}\right) ||\mathbf{v}_f|| \tag{3.74}$$

A time step for the initial guess trajectory is derived by dividing the time of flight guess by the index of the final trajectory node, k_f:

$$k_f = N - 1 \tag{3.75}$$

$$\Delta\tau = \frac{t_f}{k_f} \tag{3.76}$$

Using $\mu[k]$, $s[k]$ and $\Delta\tau$, an initial guess of the whole trajectory can then be produced which will form the basis upon which successive iterations will linearise. The objective function for the initial trajectory generation is defined as:

$$\underset{\mathbf{T},\Gamma}{\text{minimise}} \quad -\omega_{m,f} m[k_f] + \omega_{\kappa,\mathbf{a},R} ||\kappa_{\mathbf{a},R}|| \tag{3.77}$$

where $||\kappa_{\mathbf{a},R}||$ is a parameter which serves to limit the magnitude of any artificial accelerations that act on the vehicle if the linearisation process generates artificial infeasibility, and $\omega_{m,f}$ and $\omega_{\kappa,\mathbf{a},R}$ are positive weighting parameters.

The convexified constraints are applied:

$$m_{dry} \leq m[k] \tag{3.78}$$

$$||\mathbf{r}[k]|| \cos(\gamma_{gs}) \leq \hat{\mathbf{e}}_u^\top \mathbf{r}[k] \tag{3.79}$$

$$||\mathbf{T}[k]|| \leq \Gamma[k] \tag{3.80}$$

$$0 \leq T_{min} \leq \Gamma[k] \leq T_{max} \tag{3.81}$$

$$\Gamma[k] \cos(\theta_{max}) \leq \hat{\mathbf{e}}_u^\top \mathbf{T}[k] \tag{3.82}$$

$$\dot{T}_{min}\Delta\tau \leq \Gamma[k+1] - \Gamma[k] \leq \dot{T}_{max}\Delta\tau \tag{3.83}$$

And the linear dynamics:

$$m[k+1] = m[k] - \left[\frac{\alpha}{2}\left(\Gamma[k] + \Gamma[k+1]\right) + \dot{m}_{bp}\right]\Delta\tau \tag{3.84}$$

$$\mathbf{r}[k+1] = \mathbf{r}[k] + \mathbf{v}[k]\Delta\tau + \frac{1}{3}\left(\mathbf{a}[k] + \frac{1}{2}\mathbf{a}[k+1]\right)\Delta\tau^2 \tag{3.85}$$

$$\mathbf{v}[k+1] = \mathbf{v}[k] + \frac{1}{2}\left(\mathbf{a}[k] + \mathbf{a}[k+1]\right)\Delta\tau \tag{3.86}$$

$$\mathbf{a}[k] = \frac{1}{\mu[k]}\left(\mathbf{T}[k] - \frac{1}{2}\rho S_D C_D s[k]\mathbf{v}[k]\right) + \mathbf{a}_R[k] + \mathbf{g} \tag{3.87}$$

Finally, a modification is made to limit the artificial acceleration via the $\kappa_{\mathbf{a},R}[k]$ term in the objective function:

$$||\mathbf{a}_{rel}[k]|| \leq \kappa_{\mathbf{a},R}[k] \tag{3.88}$$

Successive iterations

The initialisation trajectory is then linearised around in successive iterations, until convergence. A state vector $\mathbf{\Psi}_i[k]$ is defined which contains the trajectory data at iteration iteration i:

$$\mathbf{\Psi}_i[k] \triangleq \begin{bmatrix}\Delta t & \mathbf{\Psi}_m^\top[k] & \mathbf{\Psi}_\Gamma^\top[k] & \mathbf{\Psi}_\mathbf{v}^\top[k] & \mathbf{\Psi}_\mathbf{T}^\top[k] & \mathbf{\Psi}_{\mathbf{a},R}^\top[k]\end{bmatrix}^\top \tag{3.89}$$

The linearisation process introduces a risk that the convexified problem could be rendered unbounded such that a gradient-based solver traverses the solution space in a direction that indefinitely decreases the objective function without ever encountering a constraint that stops it. Without additional constraints, solutions may move along directions where the linear approximation fails to reflect the true change in the objective function relative to the optimisation variables, thereby losing the implicit boundaries that the original non-linear constraint imposed.

To safeguard against potential unboundedness, "trust regions" are introduced. These are additional constraints that limit how far the solution at the current iteration can deviate from that of the previous iteration. Trust regions ensure that the linear approximation remains a good local representation of the untreated problem. Instead of allowing the solver to traverse to distant parts of the solution space where the linear model is inaccurate or too permissive, the trust regions serve to ensure that it stays within a neighbourhood where the linearisation is valid and where unboundedness is less likely to occur. The trust regions are defined as:

$$\delta\Delta t_i^2 \leq \eta_{\Delta t} \tag{3.90}$$

$$\delta \mathbf{T}_i^\top[k]\delta \mathbf{T}_i[k] \leq \eta_{\mathbf{T}}[k] \tag{3.91}$$

$$||\mathbf{a}_R[k]|| \leq \kappa_{\mathbf{a},R}[k] \tag{3.92}$$

where $\delta x_i[k] = x_i[k] - x_{i-1}[k]$ represents the change in the associated variable x_i evaluated at integration step k between the i and $i-1^{\text{th}}$ iterations.

The objective function for the successive iterations is given by:

$$\underset{\Delta t, \mathbf{T}, \Gamma}{\text{minimise}} \quad -\omega_{m,f} m[k_f] + \omega_{\eta,\Delta t}\eta_{\Delta t} + \omega_{\eta,\mathbf{T}}||\eta_{\mathbf{T}}|| + \omega_{\kappa,\mathbf{a},R}||\kappa_{\mathbf{a},R}|| \tag{3.93}$$

with the $\eta_{\Delta t}$ and $\eta_{\mathbf{T}}$ and their associated ω weighting parameters serving to incorporate the trust region constraints into the objective function.

The non-linear state equations are linearised by performing a first-order Taylor series expansion around the previously-obtained trajectory $\mathbf{\Psi}_{i-1}[k]$:

$$f(\mathbf{\Psi}_i[k]) \approx f(\mathbf{\Psi}_{i-1}[k]) + \left.\frac{\partial f}{\partial \mathbf{\Psi}}\right|_{\mathbf{\Psi}_{i-1}[k]} \delta \mathbf{\Psi}_i[k] \tag{3.94}$$

Where $\delta \mathbf{\Psi}_i[k] = \mathbf{\Psi}_i[k] - \mathbf{\Psi}_{i-1}[k]$ and $\frac{\partial f}{\partial \mathbf{\Psi}}$ is the Jacobian of f with respect to $\mathbf{\Psi}$. This transforms non-linear products into affine expressions in the incremental variables $\delta\Delta t$ and others, ensuring the resulting problem remains convex.

To linearise the mass reciprocal in the acceleration dynamics, a Taylor expansion is again performed around $m_{prev}[k]$. With $\delta m[k] = m[k] - m_{prev}[k]$:

$$\frac{1}{m[k]} \approx \frac{1}{m_{prev}[k]} - \frac{\delta m[k]}{m_{prev}[k]^2} \tag{3.95}$$

Since $m_{prev}[k]$ is a known constant at the current iteration, the resulting expression is affine in terms of the decision variable $m[k]$.

The drag force evaluated at the previous iteration is:

$$\mathbf{D}_{prev}[k] = -\frac{1}{2}\rho S_D C_D ||\mathbf{v}_{prev}[k]||\mathbf{v}_{prev}[k] \tag{3.96}$$

With fixed $\mathbf{v}_{prev}[k]$, the Jacobian of $\mathbf{D}[k]$ with respect to $\mathbf{v}[k]$ is computed. The first-order approximation yields:

$$\mathbf{D}[k] \approx \mathbf{D}_{prev} + \mathbf{J}_{\mathbf{D}} \cdot (\mathbf{v}[k] - \mathbf{v}_{prev}[k]) \tag{3.97}$$

where $\mathbf{J}_{\mathbf{D}}$ is the constant Jacobian matrix (computed from $\mathbf{v}_{prev}[k]$). This linear approximation of drag is then substituted back into the acceleration equation. After substitution

and collecting constants, the acceleration becomes an affine function of $\mathbf{T}[k]$ and $\mathbf{v}[k]$:

$$\mathbf{a}[k] \approx \left(\frac{1}{m_{prev}[k]} - \frac{\delta m[k]}{m_{prev}[k]^2} \right) (\mathbf{T}[k] - (\mathbf{D}_{prev}[k] + \mathbf{J_D} (\mathbf{v}[k] - \mathbf{v}_{prev}[k]))) + \mathbf{g} \quad (3.98)$$

The artificial, or relaxation, acceleration term $\mathbf{a}_{rel}[k]$ is introduced as a slack variable to handle any artificial infeasibility that might arise from the imposed linearisation. These terms are penalised in the objective function to ensure that they remain small (or zero), acting as a safety buffer to preserve feasibility while the problem iterates towards a converged solution.

3.3.6 Example Landing Trajectories

Example trajectories simulating identical vehicle configurations are provided, with initial conditions inferred from telemetry data from landings of SpaceX Falcon 9 boosters[14], the closest operational analogue to RFA TWO. The robustness of the algorithm to a range of flight conditions is illustrated by simulating a trajectory with excessive initial mass, where the algorithm provides a solution that involves the vehicle burning off excess fuel before landing successfully.

Typical landing

Figures 3.12 to 3.15 show a typical landing trajectory for the RFA TWO booster.

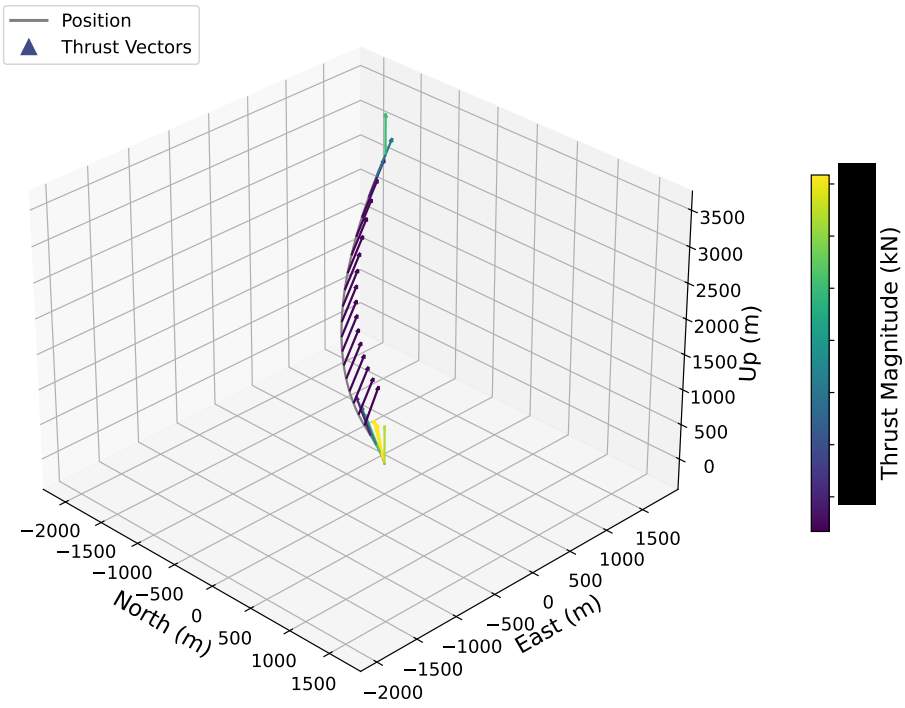

Figure 3.12: Booster position and pointwise thrust vectors for a typical landing

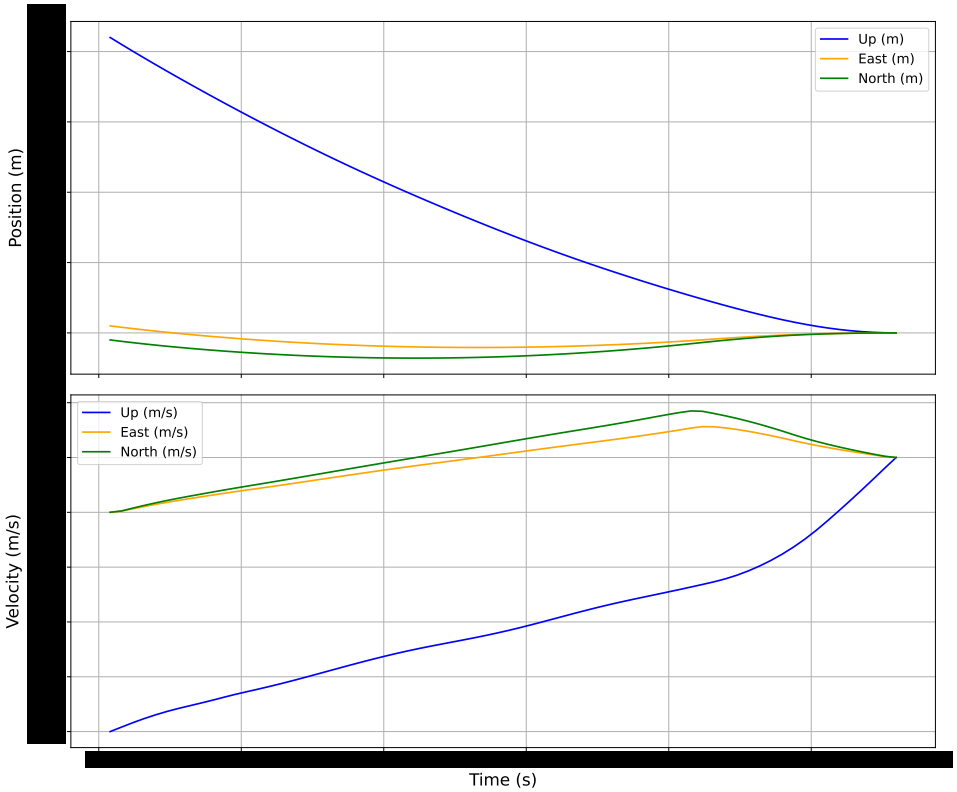

Figure 3.13: Components of booster position and velocity across a typical landing

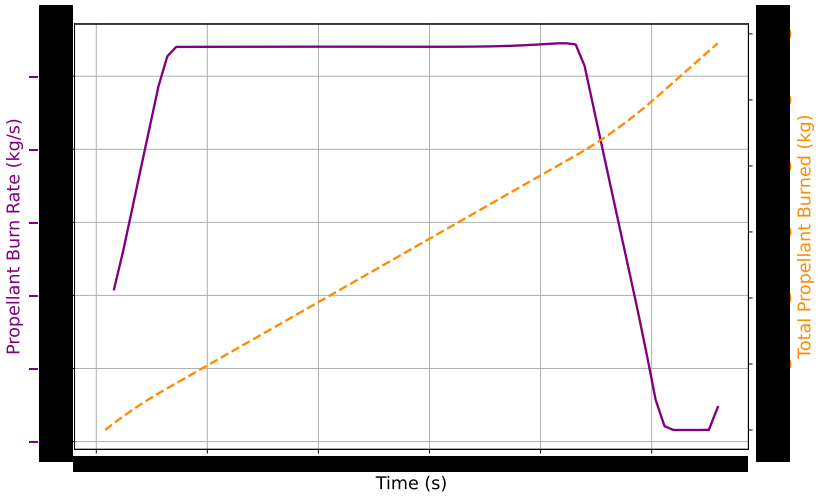

Figure 3.14: Propellant depletion for a typical landing

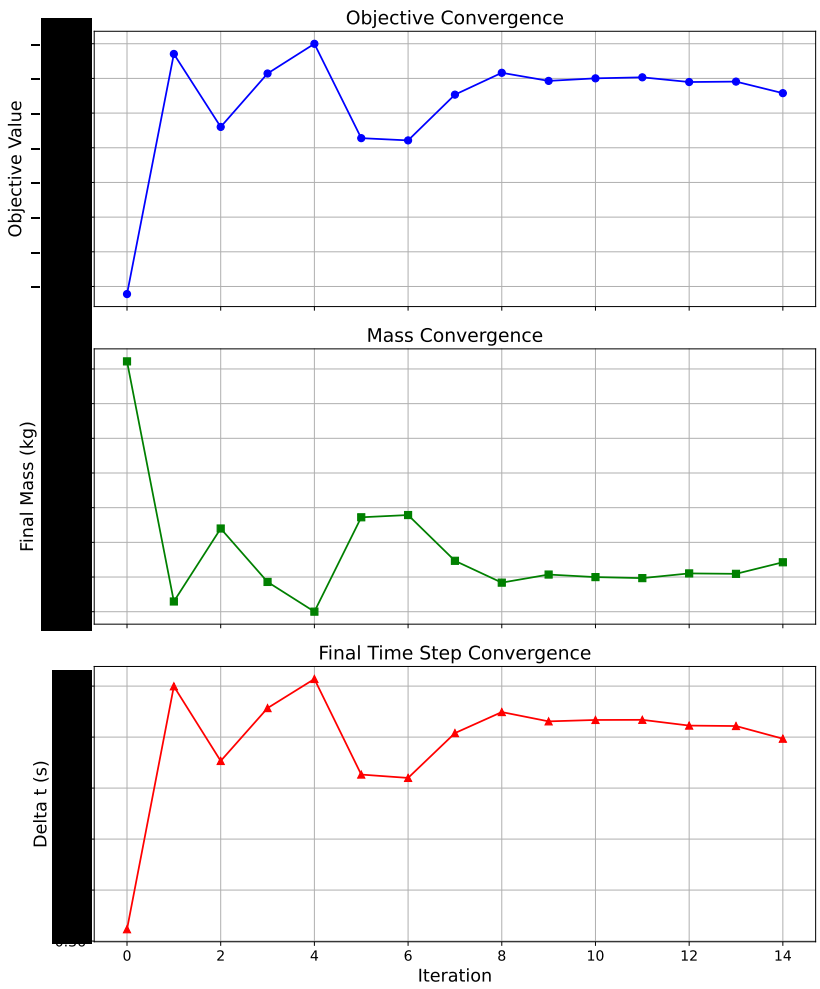

Figure 3.15: Convergence of typical landing parameters across problem iterations

Landing with excessive mass

The case of landing with excessive mass, in this case where $m_0 = 50000$ kg, is quite unrealistic. However, the example is included in Figures 3.16 to 3.18 to show that the landing algorithm is capable of successfully landing the booster even in a case where the thrust-to-weight ratio is too low to sufficiently reduce the speed before ground impact. In this hypothetical situation, it can be seen that the algorithm will guide the booster on a path such that fuel is expended until its mass becomes low enough to achieve soft landing.

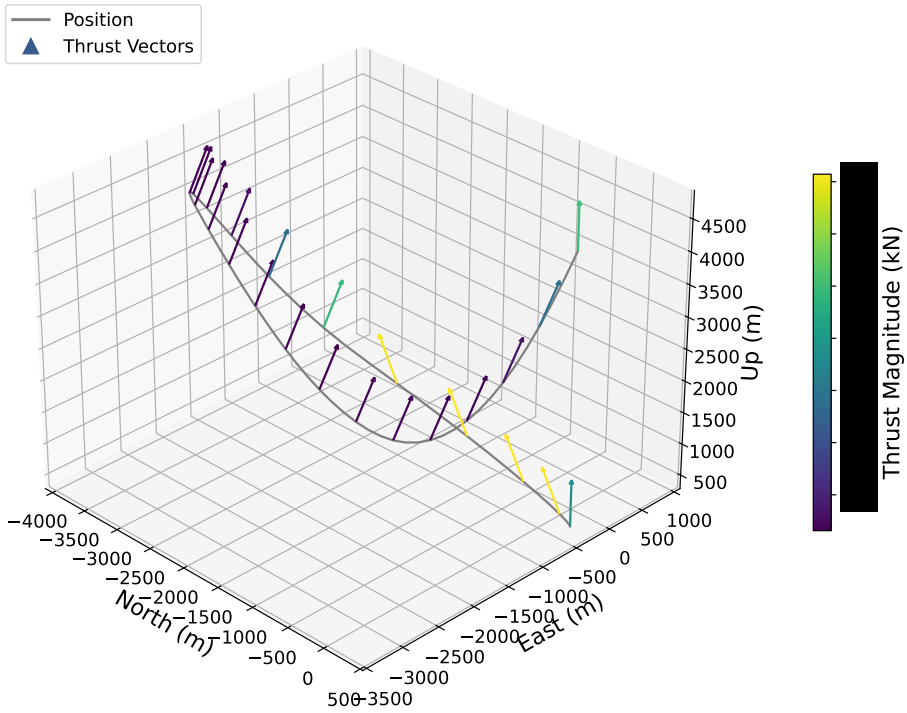

Figure 3.16: Booster position and pointwise thrust vectors for an excessive-mass landing

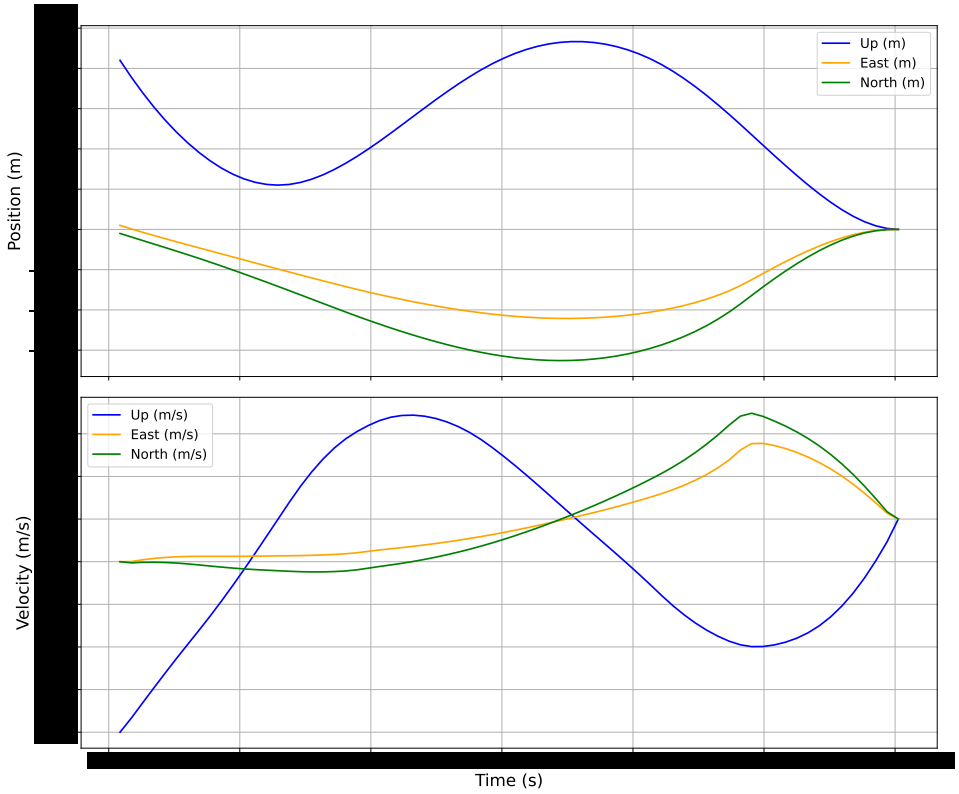

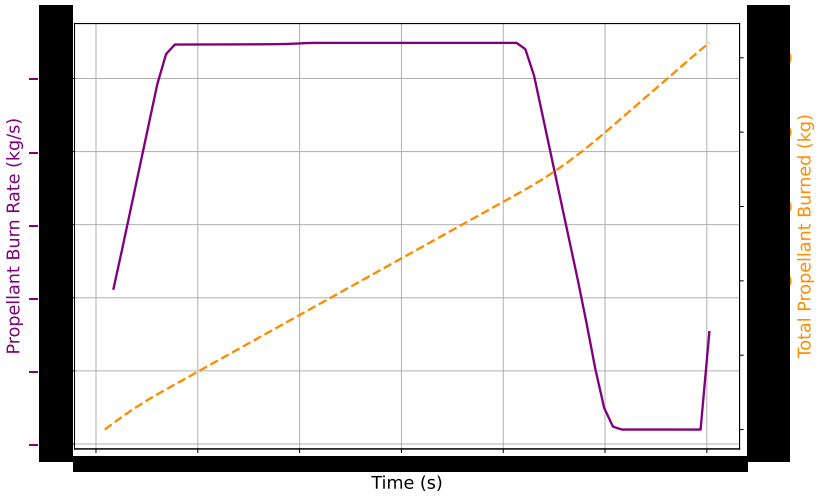

Figure 3.17: Propellant depletion for an excessive-mass landing

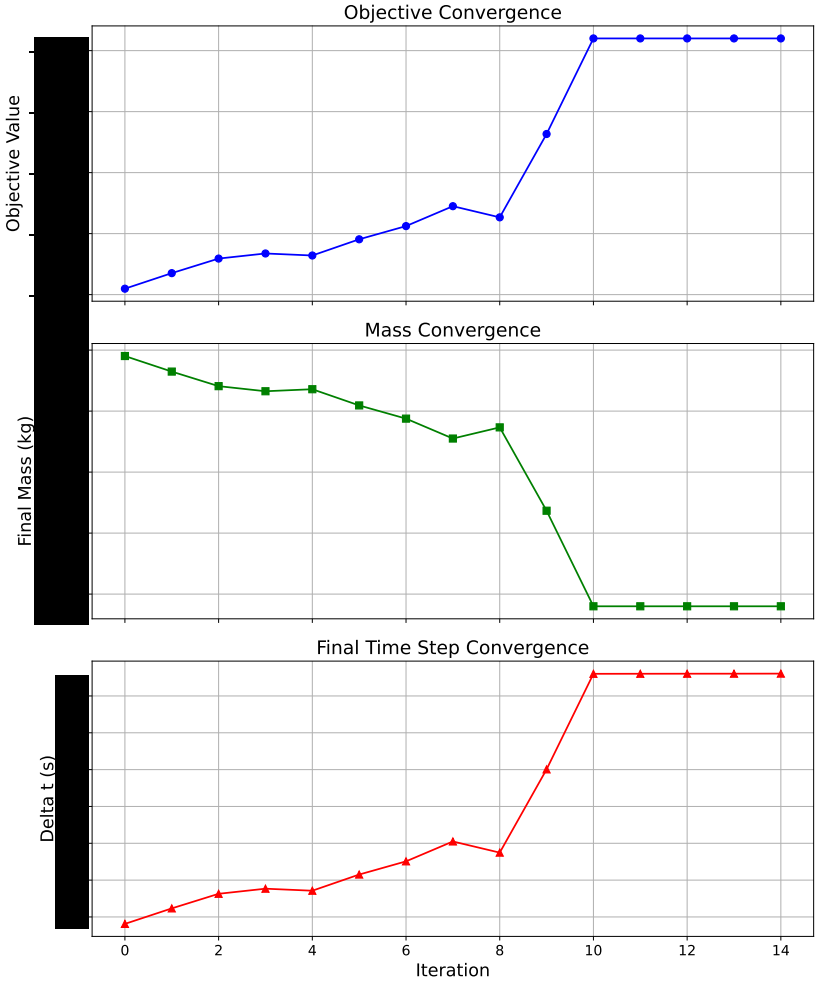

Figure 3.18: Convergence of excessive-mass landing parameters across problem iterations

4

Parametric Analysis and Design

In addition to the development of the whole-mission simulator, a secondary aim of this project was to apply the simulator to a parametric analysis and design study of the RFA TWO launch system. This section details the approach taken to conduct the study and the relevant results.

4.1 Approach

The parametric analysis and design study was conducted by performing a mission simulation using a "base configuration" of RFA TWO, observing the base configuration performance across the mission, then systematically changing the vehicle parameters within reasonable ranges to observe the effect of these changes on the performance of the launch system. Only first-order effects arising from the adjustment from the nominal case of a single vehicle parameter per simulation were assessed within the scope of this project.

4.2 Base Configuration

The base vehicle configuration stems from the output of several runs of the [redacted] tool (see Section 1.5) that were conducted by RFA prior to the commencement of this project. The boundary conditions supplied to [redacted] for generating this configuration were based on well-understood or approximate specifications of known hardware such as the [redacted] system, as well as orbital parameters of a nominal RFA TWO mission as defined by [redacted]. Many parameters, especially those related to the landing phase of the mission, were not considered at the time at which the [redacted] were carried out by RFA. In order to simulate the [redacted] base configuration using the simulator from this project, empirically-obtained values for boundary conditions or constraints were applied in some cases. For example, the recovery and RCS hardware and mass parameters are defined based on empirical

data, with the total mass properties of the vehicle augmented accordingly. The resulting base configuration parameters are displayed in Tables 4.1 to 4.5

Table 4.1: RFA TWO base configuration mission parameters

Mission parameter	**Value**
Launch site	[redacted] °N, [redacted] °W
Nominal target orbit	[redacted] km, [redacted]° i
Booster separation time	burn + [redacted] s
[redacted] time	burn + [redacted] s
[redacted] time	burn + [redacted] s

Table 4.2: RFA TWO base configuration general vehicle parameters

Vehicle parameter	**Value**
Gross lift-off mass	[redacted] kg
Propellant mass	[redacted] kg
Inert mass	[redacted] kg
Ideal payload mass for nominal orbit	[redacted] kg
Margined payload mass for nominal orbit	[redacted] kg
Fairing mass	[redacted] kg
Diameter	[redacted] m
Length	[redacted] m
Fairing length	[redacted] m
Frontal reference area	[redacted] m^2
Initial thrust-to-weight ratio	[redacted]
Dynamic pressure limit	[redacted]
Maximum pitch rate	[redacted] °/s
Maximum acceleration	[redacted] m/s^2

Table 4.3: RFA TWO base configuration booster parameters

Booster parameter	**Value**
Lift-off mass	[redacted] kg
Propellant mass (including unburnt propellant)	[redacted] kg
Usable propellant mass	[redacted] kg
Inert mass	[redacted] kg
[redacted]	[redacted]
[redacted] mass	[redacted] kg
[redacted]	[redacted] %
Length	[redacted] m
Total number of engines	[redacted]
Number of engines [redacted]	[redacted]
Engine gimbal half-angle	[redacted] °
Combined nozzle exit area	[redacted] m^2
Burn time	[redacted] s
Sea level thrust	[redacted] kN
Vacuum thrust	[redacted] kN
Thrust magnitude rate limit	± [redacted]
Vacuum specific impulse	[redacted] s
Throttle depth	[redacted]
Total [redacted] thrust	[redacted] N
[redacted]	[redacted] m
[redacted]	[redacted] m
Centre of mass distance from base	[redacted] m
Transverse moment of inertia at manoeuvre	[redacted] $kg \cdot m^2$
Staging altitude	[redacted] km
[redacted]	[redacted] m
[redacted]	[redacted] ° from azimuth

Table 4.4: RFA TWO base configuration [redacted] parameters

[redacted] **parameter**	**Value**
Lift-off mass	[redacted] kg
Propellant mass (including unburnt propellant)	[redacted] kg
Usable propellant mass	[redacted] kg
Inert mass	[redacted] kg
Length	[redacted] m
Number of engines	[redacted]
Combined nozzle exit area	[redacted] m^2
Burn time	[redacted] s
Vacuum thrust	[redacted] kN
Vacuum specific impulse	[redacted] s
Nominal Delta-V	[redacted] m/s
[redacted] altitude	[redacted] km

Table 4.5: RFA TWO base configuration [redacted] parameters

[redacted] **parameter**	**Value**
Lift-off mass	[redacted] kg
Propellant mass (including unburnt propellant)	[redacted] kg
Usable propellant mass	[redacted] kg
Inert mass	[redacted] kg
Length	[redacted] m
Number of engines	[redacted]
Combined nozzle exit area	[redacted] m^2
Burn time	[redacted] s
Vacuum thrust	[redacted] kN
Vacuum specific impulse	[redacted] s
Nominal Delta-V	[redacted] m/s
[redacted] altitude	[redacted] km

4.3 Parametric Analysis

With the base configuration defined, an analysis was carried out to assess the performance of the system. Following this, parameters were tweaked to observe the resulting impact.

4.3.1 Base Configuration Performance

Ascent

The value of h_{turn} selected by the ascent module to achieve a [redacted] km staging altitude as defined by the base [redacted] configuration is [redacted] m. The corresponding staging speed is just [redacted] m/s with the full payload mass, likely not sufficient to reach the desired orbit. The resulting trajectory is shown in Figure 4.1

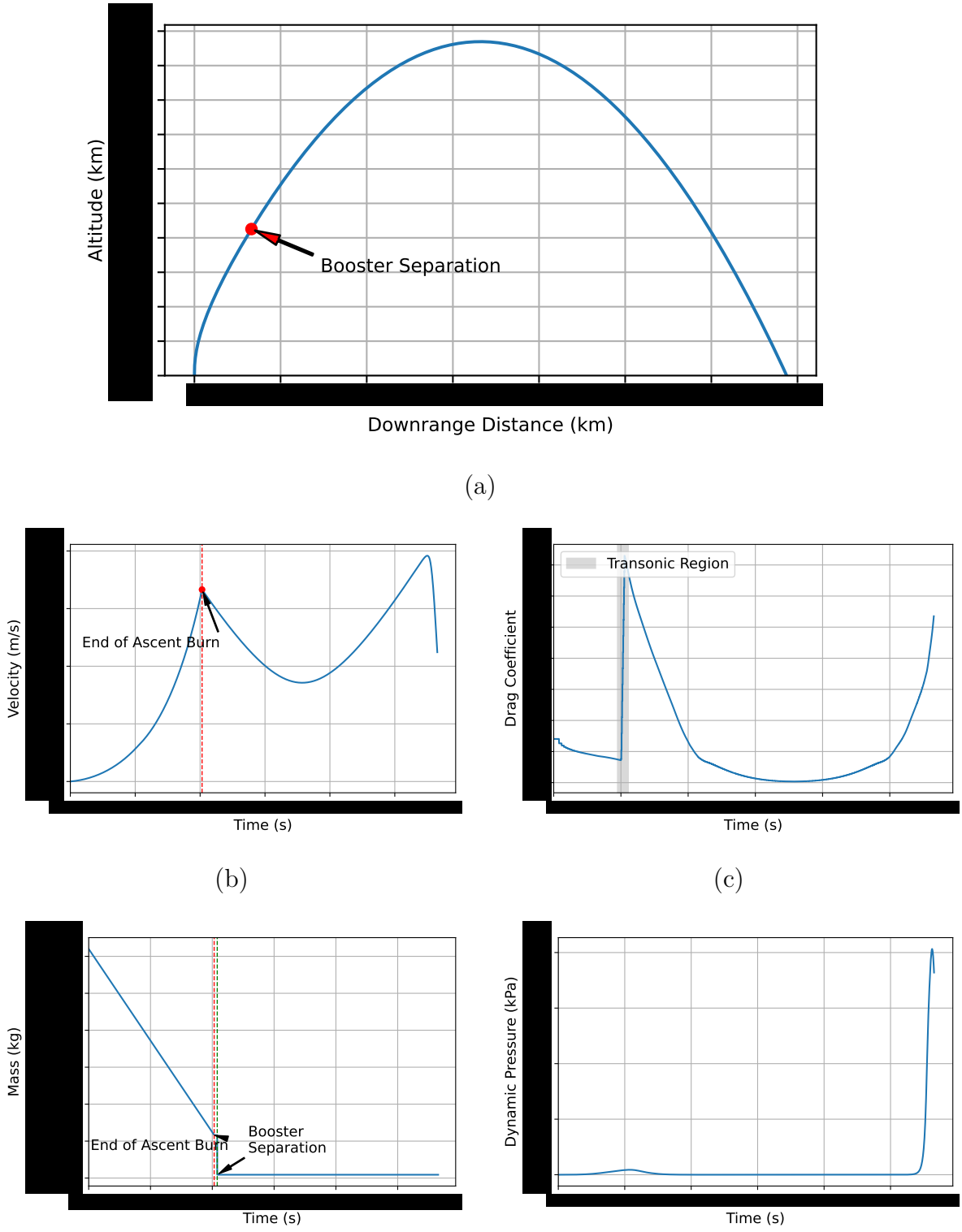

Figure 4.1: RFA TWO base configuration ballistic booster trajectory

Manoeuvre

With appropriate PID controller gains, the base configuration performs adequately in manoeuvre, reaching the target attitude in the allotted time.

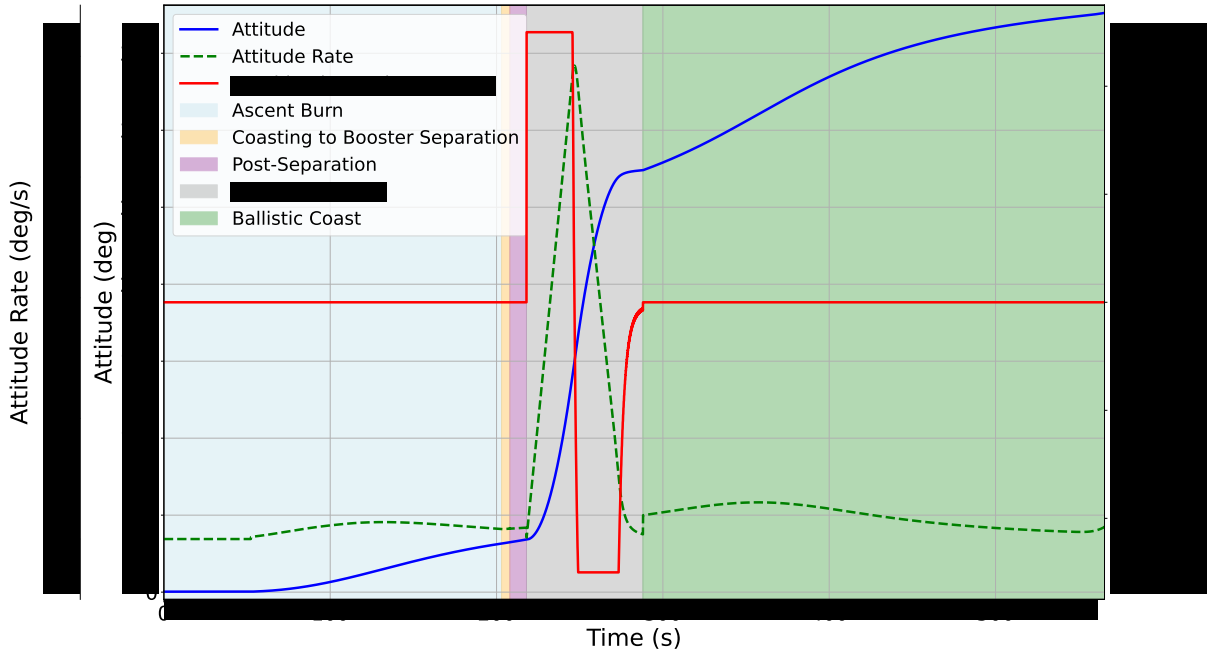

Figure 4.2: RFA TWO base configuration manoeuvre profile and combined RCS thrust application

Landing

As can be seen from Figures 4.5 to 4.5, the base configuration is capable of performing a successful landing, spanning under 35 seconds from landing burn ignition to termination and consuming around 6000 kg of propellant. The primary observation in this case is that the 10 % propellant reserve allocated for landing could be decreased, since less than a quarter is consumed.

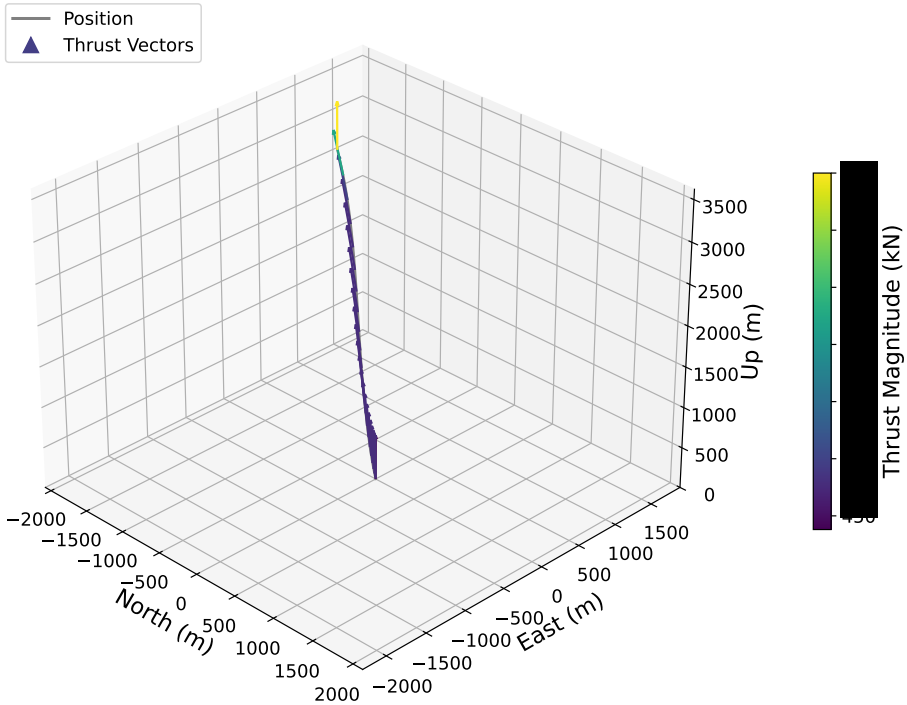

Figure 4.3: Booster position and pointwise thrust vectors for landing of the RFA TWO base configuration

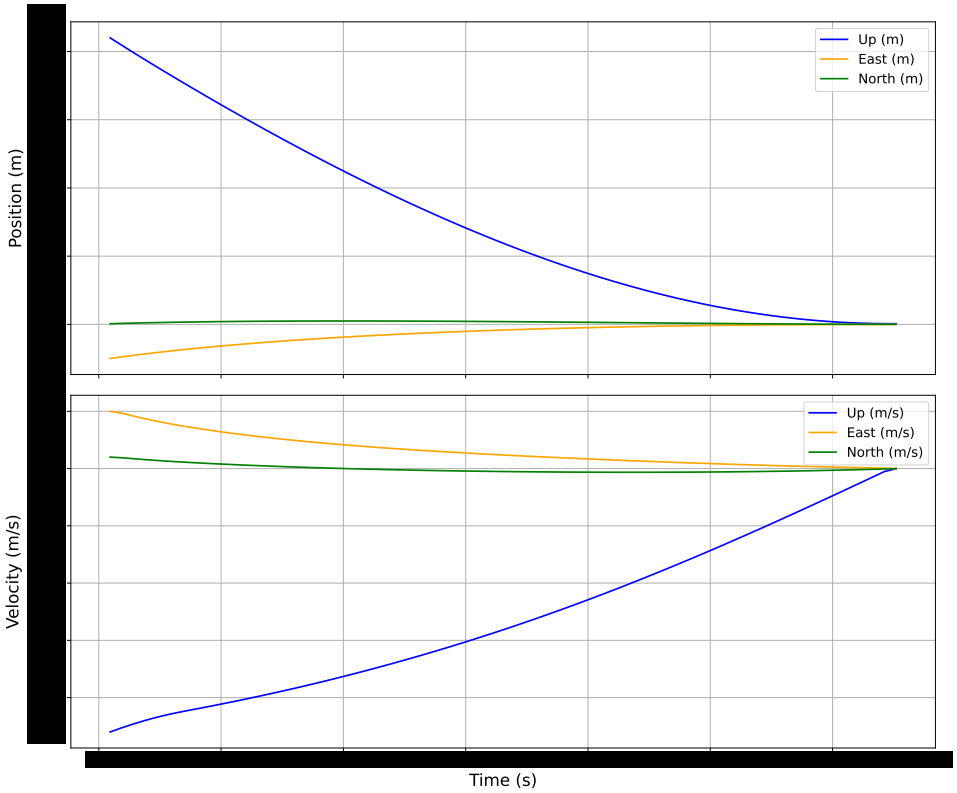

Figure 4.4: Components of booster position and velocity across the landing of the RFA TWO base configuration

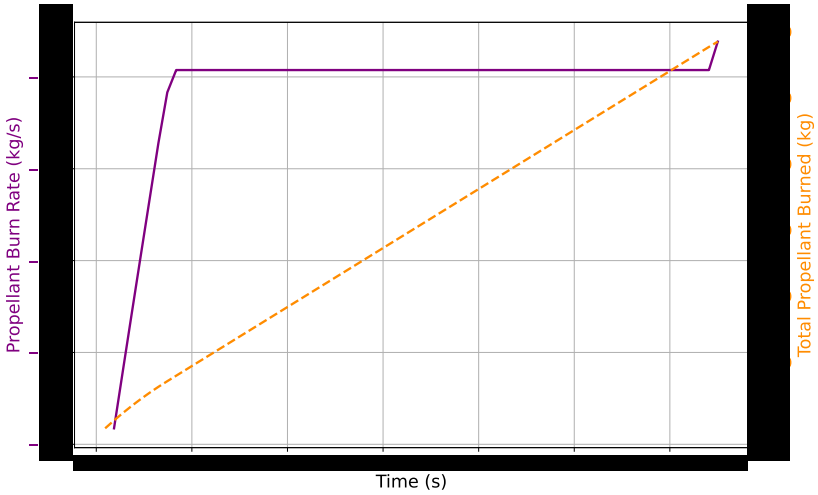

Figure 4.5: Propellant depletion for landing of the RFA TWO base configuration

4.3.2 Parameter Adjustments

A list of parameters were selected to be assessed as part of the analysis and design study, with each parameter was adjusted by ±10% and the corresponding performance impact recorded. The parameters and results are provided in Table 4.6, where 'Prop' indicates propellant consumption change, 'MSV' indicates maximum staging velocity change, and [redacted].

Table 4.6: Parameter adjustments from and results of parametric analysis and design study

Parameter	**Base configuration value**	**+10% performance impact**	**-10% performance impact**
Booster diameter	[redacted] m	Prop: +[redacted]%, MSV: +[redacted]%, [redacted]: +[redacted]%	Prop: -[redacted]%, MSV: -[redacted]%, [redacted]: -[redacted]%
Booster length	[redacted] m	Prop: +[redacted]%, MSV: +[redacted]%, [redacted]: +[redacted]%	Prop: -[redacted]%, MSV: -[redacted]%, [redacted]: -[redacted]%
Booster inert mass	[redacted] kg	Prop: +[redacted]%, MSV: -[redacted]%, [redacted]: +[redacted]%	Prop: -[redacted]%, MSV: +[redacted]%, [redacted]: -[redacted]%
Booster maximum acceleration	[redacted] m/s^2	Prop: -[redacted]%, MSV: +[redacted]%, [redacted]: -[redacted]%	Prop: +[redacted]%, MSV: -[redacted]%, [redacted]: +[redacted]%
Recovery hardware mass	[redacted] kg	Prop: +[redacted]%, MSV: -[redacted]%, [redacted]: +[redacted]%	Prop: -[redacted]%, MSV: +[redacted]%, [redacted]: -[redacted]%
Landing propellant reserve	[redacted]%	Prop: +[redacted]%, MSV: [redacted]%, [redacted]: +[redacted]%	Prop: -[redacted]%, MSV: [redacted]%, [redacted]: -[redacted]%
Engine gimbal half-angle	[redacted]°	Prop: -[redacted]%, MSV: +[redacted]%, [redacted]: +[redacted]%	Prop: +[redacted]%, MSV: -[redacted]%, [redacted]: -[redacted]%
Transverse moment of inertia	[redacted] $kg \cdot m^2$	Prop: +[redacted]%, MSV: [redacted]%, [redacted]: +[redacted]%	Prop: -[redacted]%, MSV: [redacted]%, [redacted]: -[redacted]%
Booster staging altitude	[redacted] km	Prop: -[redacted]%, MSV: +[redacted]%, [redacted]: [redacted]%	Prop: +[redacted]%, MSV: -[redacted]%, [redacted]: [redacted]%
Landing burn initiation altitude	[redacted] m	Prop: +[redacted]%, MSV: [redacted]%, [redacted]: +[redacted]%	Prop: -[redacted]%, MSV: [redacted]%, [redacted]: -[redacted]%

4.3.3 Advisory Design Changes

Based on the estimated impacts provided in Table 4.6, a list of suggested advisory design changes for the RFA TWO launch system are provided. The rationale emphasises minimisation of propellant consumption and manoeuvre time, whilst considering maximum staging velocity when relevant. In cases where both changes lead to undesirable outcomes or the difference is minimal, the option resulting in the greatest propellant savings is preferred.

- **Booster diameter:** Decreasing by 10% reduces propellant usage by about [redacted]% and [redacted] time by [redacted]%, making it favourable compared to increasing diameter, which increases propellant and [redacted] time. [redacted]
- **Booster length:** Reducing length by 10% yields a propellant saving of [redacted]% and a slight reduction in [redacted] time, whereas increasing length worsens both. [redacted]
- **Booster inert mass:** A lighter booster (−10%) saves [redacted]% propellant and reduces [redacted] time. Increasing mass is detrimental. [redacted]
- **Booster maximum acceleration:** Increasing max acceleration (+10%) improves propellant usage ([redacted]%) and reduces [redacted] time ([redacted]%), making it preferable to reducing acceleration. [redacted]
- **Recovery hardware mass:** Lighter recovery hardware (−10%) lowers propellant consumption by [redacted]% and slightly reduces [redacted] time, whereas increasing it raises both. [redacted]
- **Landing propellant reserve:** Decreasing the reserve (−10%) saves about [redacted]% propellant and reduces [redacted] time compared to increasing the reserve, which adds propellant consumption. [redacted]
- **Engine gimbal half-angle:** Increasing gimbal angle (+10%) saves [redacted]% propellant, although [redacted] time rises slightly. Decreasing angle does the opposite. Prioritising propellant savings, [redacted]
- **Transverse moment of inertia:** Decreasing the MoI (−10%) cuts propellant consumption ([redacted]%) and [redacted] time ([redacted]%). Increasing it worsens both. [redacted]
- **Booster staging altitude:** Higher staging altitude (+10%) saves propellant ([redacted]%) without changing [redacted] time. Lower altitude adds propellant consumption. [redacted]

- **Landing burn initiation altitude:** Lower altitude (-10%) reduces propellant consumption ([redacted]%) and [redacted] time ([redacted]%), while higher altitude increases both. [redacted]

Of course, it is obvious that simply changing a parameter by 10% in any direction is non-trivial, and higher-order effects of one parameter change on another are not considered, which is a highly reductive assumption. Regardless, it is clear from this demonstrative analysis that the simulator developed in this project can generate insightful results to inform the design direction of the RFA TWO launch system.

5

Limitations and Future Work

The aerodynamic deceleration phase of flight is not fully considered, which is a limitation and should be incorporated in future efforts. Since the aerodynamic deceleration phase does not deplete mass, the simulator still characterises the performance of the vehicle effectively. However, the use of aerodynamic control surfaces can reduce vehicle velocity beyond what would be expected from pure ballistic re-entry and can position the booster closer to the landing site, potentially resulting in less energy expenditure via propellant consumption in the retro-propulsive landing burn.

Distinction is not made in this project between so-called 'downrange' and 'return-to-launch-site' (RTLS) concepts of operations for booster recovery. It turns out that the landing algorithm from this project performs well in guiding the vehicle from any initial state to any final state subject to vehicle and mission boundary conditions, including cases where the final state is not at ground level. This feature is suitable for analysis and simulation of the 'boostback burn' associated with RTLS regimes, and future work would include further assessment in this domain.

Finally, due to constraints on high-performance computing resources over the course of this project, landing profiles could not be effectively compared against [redacted]. Such comparisons would be interesting for future efforts and would assist in highlighting the value of this project.

Bibliography

[1] Rocket Factory Augsburg AG, Rfa one, Accessed: 2024-12-20, 2024. [Online]. Available: https://www.rfa.space/rfa-one/.

[2] SaxaVord Spaceport, Saxavord spaceport, Accessed: 2024-12-20, 2024. [Online]. Available: https://saxavord.com/.

[3] YouTube, Helix engine - full length hot fire test - technical feed, Accessed: 2024-12-20, 2024. [Online]. Available: https://www.youtube.com/watch?v=MXUR4m6SOB0.

[4] Rocket Factory Augsburg AG, Redshift, Accessed: 2024-12-20, 2024. [Online]. Available: https://www.rfa.space/redshift/.

[5] Rocket Factory Augsburg AG, Argo, Accessed: 2024-12-20, 2024. [Online]. Available: https://www.rfa.space/argo/.

[6] Eurospace, "SpaceX Launch Service Economics," Eurospace, Tech. Rep., 2021, Research paper. [Online]. Available: https://spacetransportation.esa.int/.

[7] National Aeronautics and Space Administration, NASA Systems Engineering (NASA SP-2016-6105), Rev 2. Washington, DC: NASA, 2016, ch. 3, Chapter 3: NASA Program/Project Life Cycle Standards. [Online]. Available: https://www.nasa.gov.

[8] European Space Agency, Europe's spaceport, Accessed: 2024-12-20, 2024. [Online]. Available: https://www.esa.int/Enabling_Support/Space_Transportation/Europe_s_Spaceport/Europe_s_Spaceport2.

[9] U.S. Naval Research Laboratory, NRLMSISE-00 Atmospheric Model, Accessed: 2024-12-20, 2024. [Online]. Available: https://map.nrl.navy.mil/map/pub/nrl/NRLMSIS/NRLMSISE-00/.

[10] C. E. Rogers and D. Cooper, RASAero II Aerodynamic Analysis, Developed by Rogers Aeroscience. Accessed: 2024-12-20, 2024. [Online]. Available: https://www.rasaero.com/.

[11] R. D. Finck, "USAF Stability and Control DATCOM," McDonnell Douglas Corporation, Douglas Aircraft Division, Long Beach, California, Final Report AFWAL-TR-83-3048, 1978, Distribution limited to U.S. Government agencies only; Official/-Operational Use; March 1982. Other requests must be referred to AFWAL/FIGC, Wright-Patterson AFB, Ohio 45433. Subject to export control laws.

[12] M. Szmuk, B. Açıkmeşe, and A. W. B. Jr., "Successive convexification for fuel-optimal powered landing with aerodynamic drag and non-convex constraints," in AIAA Guidance, Navigation, and Control Conference, American Institute of Aeronautics and Astronautics, San Diego, California, USA, 2016. DOI: 10.2514/6.2016-0378.

[13] S. Diamond and S. Boyd, "CVXPY: A Python-embedded modeling language for convex optimization," Journal of Machine Learning Research, 2016, To appear. [Online]. Available: https://stanford.edu/~boyd/papers/pdf/cvxpy_paper.pdf.

[14] Flight Club, Sentinel-6 launch with simulated telemetry, https://www.youtube.com/watch?v=1BYi2_8cBvw, Accessed: 2024-11-06, 2020.